(4)

AFGL-TR-89-0085

Effects of a Descending Lithospheric Slab on Yield Estimates of Underground Nuclear Tests

Vernon F. Cormier
Woohan Kim

The University of Connecticut
Department of Geology and Geophysics
345 Mansfield Road
Storrs, Connecticut 06269-2045

28 February 1989

Semi-Annual Report No. 1

AIR FORCE GEOPHYSICS LABORATORY
AIR FORCE SYSTEMS COMMAND
UNITED STATES AIR FORCE
HANSCOM AIR FORCE BASE, MASSACHUSETTS 01731-5000

SPONSORED BY
Defense Advanced Research Projects Agency
Nuclear Monitoring Research Office
ARPA ORDER NO. 5299

MONITORED BY
Geophysics Laboratory
Contract No. F19628-88-K-0010

This technical report has been reviewed and is approved for publication.

JAMES F. LEWKOWICZ
Contract Manager
Solid Earth Geophysics Branch
Earth Sciences Division

JAMES F. LEWKOWICZ
Branch Chief
Solid Earth Geophysics Branch
Earth Sciences Division

FOR THE COMMANDER

DONALD H. ECKHARDT, Director
Earth Sciences Division

This report has been reviewed by the ESD Public Affairs Office (PA) and is releasable to the National Technical Information Service (NTIS).

Qualified requestors may obtain additional copies from the Defense Technical Information Center. All others should apply to the National Technical Information Service.

If your address has changed, or if you wish to be removed from the mailing list, or if the addressee is no longer employed by your organization, please notify AFGL/DAA, Hanscom AFB, MA 01731-5000. This will assist us in maintaining a current mailing list.

Do not return copies of this report unless contractual obligations or notices on a specific document requires that it be returned.

UNCLASSIFIED

SECURITY CLASSIFICATION OF THIS PAGE

REPORT DOCUMENTATION PAGE

Form Approved
OMB No 0704-0188

1a REPORT SECURITY CLASSIFICATION Unclassified	1b RESTRICTIVE MARKINGS
2a SECURITY CLASSIFICATION AUTHORITY	3 DISTRIBUTION/AVAILABILITY OF REPORT Approved for public release; distribution unlimited
2b DECLASSIFICATION/DOWNGRADING SCHEDULE	
4 PERFORMING ORGANIZATION REPORT NUMBER(S)	5 MONITORING ORGANIZATION REPORT NUMBER(S) AFGL-TR-89-0085
6a NAME OF PERFORMING ORGANIZATION The University of Connecticut 6b OFFICE SYMBOL (If applicable)	7a NAME OF MONITORING ORGANIZATION Air Force Geophysics Laboratory
6c ADDRESS (City, State, and ZIP Code) Geology and Geophysics 345 Mansfield Road, Room 207, Beach Hall The University of Connecticut Storrs, Connecticut 06269-2045	7b ADDRESS (City, State and ZIP Code) Hanscom Air Force Base Massachusetts 01731-5000
8a NAME OF FUNDING SPONSORING ORGANIZATION Defense Advanced Research Projects Agency 8b OFFICE SYMBOL (If applicable) NMRO	9 PROCUREMENT INSTRUMENT IDENTIFICATION NUMBER Contract #F 19628-88-K-0010
8c ADDRESS (City, State, and ZIP Code) 1400 Wilson Boulevard Arlington, Virginia 22209-2308	10 SOURCE OF FUNDING NUMBERS PROGRAM ELEMENT NO: 6/10/E; PROJECT NO: 8A10; TASK NO: DA; WORK UNIT ACCESSION NO: AE

11 TITLE (Include Security Classification)
Effects of a Descending Lithospheric Slab on Yield Estimates of Underground Nuclear Tests

12 PERSONAL AUTHOR(S)

13a TYPE OF REPORT	13b TIME COVERED	14 DATE OF REPORT (Year, Month, Day)	15 PAGE COUNT
Semi-Annual Report No. 1	FROM 03/08/88 TO 09/07/88	1989, February 28	54

16 SUPPLEMENTARY NOTATION

17 COSATI CODES		
FIELD	GROUP	SUB-GROUP

18 SUBJECT TERMS (Continue on reverse if necessary and identify by block number)
Seismic Wavefields, vicinity ray tracing system, Hamiltonian of a ray.

19 ABSTRACT (Continue on reverse if necessary and identify by block number)

A method for computing seismic wavefields in a high frequency approximation is proposed based on the integration of the kinematic ray tracing equations and a new set of differential equations for the dynamic properties of the wavefront, which we call the vicinity ray tracing equations. These equations are directly obtained from the Hamiltonian of a ray in ray centered coordinates, using no paraxial approximations. This system is comparable to the standard dynamic ray tracing system, but it is specified by fewer equations (4 versus 8 in three-dimensions) and only requires the specification of velocity and its first spatial derivative along a ray. The vicinity ray tracing equations define the locus of a ray in the neighborhood of the central ray. The path of the vicinity ray is predicted using properties of the medium along the vicinity ray rather than properties of the medium along the central ray. Gaussian beams are defined by assigning a Gaussian distribution of amplitude to each central ray. The width of the Gaussian is taken to be the Fresnel volume surrounding the central ray, estimated from the frequency and the distance of the vicinity ray from the central ray. Because no paraxial approximations are made, the superposition of the Gaussian

20 DISTRIBUTION/AVAILABILITY OF ABSTRACT ☐ UNCLASSIFIED/UNLIMITED ☐ SAME AS RPT ☐ DTIC USERS	21 ABSTRACT SECURITY CLASSIFICATION Unclassified
22a NAME OF RESPONSIBLE INDIVIDUAL James Lewkowicz	22b TELEPHONE (Include Area Code) 617-377-3028 22c OFFICE SYMBOL AFGL/LWH

DD Form 1473, JUN 86 Previous editions are obsolete SECURITY CLASSIFICATION OF THIS PAGE

Continuation....

19. Abstract

beams defined from vicinity rays will exhibit a much slower breakdown in accuracy as the scale length of the medium given by $\frac{v}{\nabla v}$ approaches the beamwidth.

Since second spatial derivatives of velocity are not required by the new technique, parameterization of the medium is simplified, and reflection and transmission of beams can be calculated by applying Snell's law to both vicinity rays and central rays.

TABLE OF CONTENTS

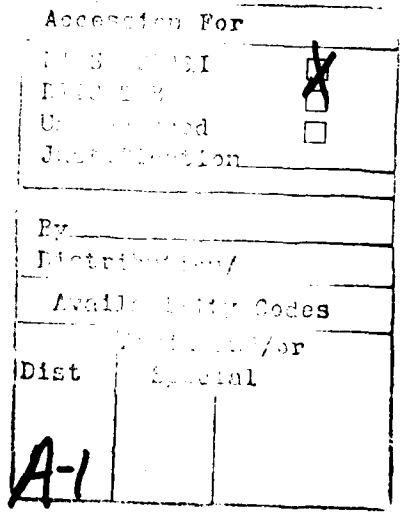

TECHNICAL SUMMARY

The objective of this project is to determine the yield bias of underground nuclear tests induced by the presence of a high velocity descending slab beneath the test site. Specifically, the effect of the Aleutian slab is being investigated on the US underground tests Longshot, Milrow, and Cannikan. P wave seismograms will be synthesized using dynamic ray tracing and superposition of Gaussian beams in three-dimensional models of the Aleutian slab determined from P travel time delays. Focusing and defocusing and multipathing at teleseismic distances will be evaluated by comparison of observed with synthetic seismograms of the Aleutian tests.

The slab problem requires that accurate body waves be synthesized for three dimensional source-receiver geometries in a three-dimensionally varying Earth model. The rapid variation of Earth structure in the vicinity of the slab requires care in assessing the validity and appropriateness of applying asymptotically approximate techniques of synthesizing body waveforms. During the first six months of the project, we have developed an improved method of dynamic ray tracing and Gaussian beam synthesis for application to this problem. The improved method does not make any paraxial approximations and defines beamwidth in terms of a Fresnel volume. By avoiding the paraxial approximation, we seek to develop a beam method that will remain valid in rapidly varying Earth models up to the point at which asymptotic ray theory fails. The conventional dynamic ray tracing and beam superposition method breaks down as the beam width approaches the scale length of the medium, which may be long before ray theory itself breaks down.

The Fresnel beamwidth criterion has been tested for diffraction from caustics by comparison with the predictions from WKBJ seismograms. Although the diffraction predicted by WKBJ seismograms is also an approximation, it is appropriate to compare the two techniques since both techniques are developed using an equivalent level of asymptotic approximation. Good agreement is obtained between the modified beam method and WKBJ seismograms for a simple model consisting of a gradient discontinuity.

1 Introduction

Many high frequency asymptotic solutions of the wave equation have been developed as effective tools for computing wave fields in inhomogeneous three dimensional media. Two of the most widely applied are the WKBJ/Maslov method (Chapman, 1978; Chapman and Drummond, 1982) and the Gaussian beam method (Babich 1980; Popov, 1982; Červený et al., 1982; and Červený and Pšenčík, 1983). Both of these techniques estimate the kinematic and dynamic properties of a wavefront from approximate solutions to the elastodynamic wave equation based on ray theory. The superposition techniques of Gaussian beams and WKBJ plane waves as well as their stationary phase approximation in geometric ray theory all require similar amplitude and weighting functions. These amplitude functions can be found by integrating a system of equations known as the dynamic ray tracing equations.

The dynamic ray tracing equations can be derived from either the eikonal equation by substitution of a paraxial approximation (Červený and Hron, 1980; Červený, 1985), or from the parabolic wave equation (Červený et al., 1982; Popov, 1982; Červený and Pšenčík, 1983). The dynamic ray tracing equations, however, have both limitations and complications. The limitations are associated with the use of the paraxial approximation, and the complications are due to the use of multiple coordinate systems.

The limitations associated with the paraxial approximation are exhibited whenever the dynamic ray tracing equations are used to estimate the travel time and amplitude at a point in the neighborhood of ray from a second order Taylor expansion of the wavefront at a point along the ray. The Taylor expansion is the essential step in the definition of Gaussian beams and paraxial rays. The region in which the error of this Taylor expansion remains below some specified threshold is generally referred to as the paraxial vicinity. The fundamental problem with the paraxial approximation is that it is not simple to specify the spatial bounds of the paraxial vicinity in a three-dimensionally varying model. In general, one must not attempt to evaluate the Taylor expansion too far from the central ray, but it is unknown how the error grows away from the central ray.

The complications associated with the use of two coordinate systems are best appreciated by considering the most general case of a three-dimensionally varying medium. In three-dimensionally varying media, the usual approach

is to specify the dynamic ray tracing equations using two coordinate systems: ray coordinates, usually consisting of the take-off angles at the source, and ray centered coordinates, consisting of a orthogonal curvilinear system that moves along with the ray (figure 1). The use of two coordinate systems, while having the advantage of converting a non-linear Ricatti equation into a system of linear equations, increases the number of equations needed to describe the quantities affecting the amplitude of the wavefield. In either the fixed Cartesian or ray centered coordinates, the standard dynamic ray tracing equations require the specification of the second spatial derivatives of velocity along a ray. This either forces the model to be parameterized with continuous first derivatives of velocity or complicates the integration by requiring jump conditions on the dynamic quantities. These jump conditions are obtained by matching the paraxially estimated phase on either side of the discontinuity in gradient (Červený and Hron, 1980; Červený, 1985).

In this paper, we develop a new system of dynamic tracing equations and Gaussian beams that eliminates many of these problems. This system is derived from the Hamiltonian of a ray. We will define a "vicinity ray" to be a ray in the neighbourhood of the central ray. Each vicinity ray has slightly different initial take-off angles with respect to the central ray (figure 2). The locus of the vicinity ray is not paraxially estimated from the standard dynamic ray tracing equations, but rather is determined much more precisely by integrating a new set of differential equations, which we refer to as the "vicinity ray tracing equations." Gaussian beams are defined by assigning a Gaussian distribution of amplitude to each central ray. The width of the Gaussian is taken to be the Fresnel volume surrounding the central ray. Since beamwidths are related to the Fresnel volume, diffracted wavefields can be accurately estimated by a superposition of Gaussian beams without the ambiguity associated with a freely varying beamwidth parameter.

In the following sections we first review the derivation of the standard dynamic ray tracing system and the limitations of the paraxial approximation. Next the vicinity ray tracing system is derived from the Hamiltonian of a ray, in which no paraxial approximations are made. Expressions for the travel time and wavefront curvature in the neighborhood of a central ray are derived using this system. Gaussian beams are defined using vicinity rays to approximate the Fresnel volume. Finally, seismograms are synthesized and compared in a simple one-dimensional model using the WKBJ method and superposition of Gaussian beams defined from vicinity rays.

2 Physical and mathematical system

Consider an arbitrary ray corresponding to a P-wave and introduce ray centered coordinates s, q_1, q_2 (figure 1). The orthogonal ray centered coordinate system along the central ray Ω and its computation are described in Popov and Pšenčík (1976), Pšenčík (1979), and Červený and Hron (1980). The ray centered coordinates are limited to a vicinity of the origin ($q_i = 0$) in which the central ray field is regular. In figure 1, the coordinate s measures the arclength along a central ray from an arbitrary reference point. q_1 and q_2 represent length coordinates and form a two-dimensional Cartesian coordinate system in the plane normal to Ω at O, with origin at Ω. All three components (s, q_1, q_2) in the ray centered coordinate system depend on the azimuth and vertical take-off angle (ϕ, δ). The basis of the coordinate system forms a right-handed system of the three unit vectors $\hat{t}, \hat{e}_1$ and $\hat{e}_2$ where $\hat{t}$ is the unit tangent vector to the central ray Ω.

2.1 Limitations in the dynamic ray tracing system

2.1.1 The paraxial approximation

The standard dynamic ray tracing system can be derived from either the eikonal equation (Červený and Hron, 1980; Madariaga, 1984; Červený, 1985) or from the parabolic wave equation (Popov, 1982; Červený and Pšenčík, 1983). In either derivation, a paraxial approximation is assumed at some stage, which involves a Taylor expansion of the wavefield about the central ray. This approximation and other approximations occuring in the derivation are not always applied consistently and terms are omitted without specifying validity conditions.

To illustrate the problems with the dynamic ray tracing system, let us review the derivation of the two-dimensional dynamic ray tracing equations starting from the eikonal equation. The eikonal equation in 2-D is

$$\frac{1}{h^2}\left(\frac{\partial \tau}{\partial s}\right)^2 + \left(\frac{\partial \tau}{\partial q}\right)^2 = \frac{1}{V^2} \qquad (1)$$

where $V = v(s, q)$. h is a scale factor in the ray centered coordinates and will be discussed subsequently. The travel time of a vicinity ray $\tau(s, q)$ can be

approximated at q=0 (Červený and Hron, 1980; Červený and Pšenčík, 1983; Červený, 1985) by:

$$\tau(s,q) \approx \tau(s) + \frac{1}{2}M(s)q^2 \tag{2}$$

where $\frac{\partial\tau}{\partial q} = 0$ and $M = \frac{\partial^2\tau(s)}{\partial q^2}$
From equation (2), it follows that

$$\frac{\partial\tau(s,q)}{\partial s} = \frac{\partial\tau(s)}{\partial s} + \frac{1}{2}\frac{\partial M(s)}{\partial s}q^2 = \frac{1}{v} + \frac{1}{2}M_{,s}\,q^2$$

$$\frac{\partial\tau(s,q)}{\partial q} = Mq \tag{3}$$

where $v = v(s,0)$. Substituting (3) into equation (1) and neglecting higher order terms gives

$$\frac{1}{h^2}\left(\frac{1}{v^2} + \frac{1}{v}M_{,s}\,q^2\right) + M^2q^2 = \frac{1}{V^2} \tag{4}$$

Rearrangng terms in (4) gives

$$\left(\frac{1}{h^2 v}M_{,s} + M^2\right)q^2 = \frac{1}{V^2} - \frac{1}{v^2h^2} \tag{5}$$

By expanding the velocity V to second order terms with respect to q=0,

$$V = v(s,q) \approx v + v_{,q}\,q + \frac{1}{2}v_{,qq}\,q^2, \tag{6}$$

the right side of equation (5) can be approximated by

$$\frac{1}{V^2} - \frac{1}{v^2h^2} \approx -\frac{1}{v^3}v_{,qq}\,q^2 \tag{7}$$

(Červený and Hron, 1980; Červený and Pšenčík, 1983; Červený, 1985), where $v_{,qq} = \frac{\partial^2 v}{\partial q^2}$.
The standard dynamic ray tracing system is obtained from equation (5) by using equation (7) and assuming h = 1. This gives

$$\frac{dM}{ds} + vM^2 + \frac{v_{,qq}}{v^2}q^2 = 0 \tag{8}$$

Since the derivation of the dynamic ray tracing system includes second order terms, any omitted terms must be carefully evaluated. Consider the scale factor h. The scale factor h is given by

$$h \quad 1 + \frac{v_{,q}}{v} q \tag{9}$$

Because it is assumed h 1 in equation (5), the neglected term $\frac{2v_{,q}}{v} q$ of h^2 in equation (5) must be vanishly small, i.e.,

$$\frac{2v_{,q}}{v} q \ll 1 \tag{10}$$

The condition in equation (10) describes the applicability of the dynamic ray tracing system. It says that extrapolation of the wavefield away from a central ray using the paraxial approximation will break down rapidly as the scale length of the medium increases. The extrapolation distance must be much less than the scale length of the medium. For Gaussian beams, it implies that the beam width must be much less than the scale length of the medium. This can be a severe restriction in rapidly varying models, in which the criterion for validity of ray theory (wavelength $\ll$ scale length) is still well satisfied.

The term given by the left side of the inequality (10) would also be omitted if the derivation of the dynamic ray tracing equation had instead started from the parabolic wave equation. In this case, the omission of this term can occur through the lack of internal consistency in deriving this system from the parabolic wave equation or from the eikonal equation (i.e., approximations of h that are inconsistent with estimates of asymptotic order given by wavelength/scale length).

2.1.2 The P and Q matrices and coordinate systems

Equation (8) is a non-linear ordinary differential equation of the first order Ricatti type. This equation can be solved by elementary analytical methods. Following Červený and Hron (1980), the 2 D system given by (8) can be generalized to a 3-D system of linear differential equations by introducing a 2×2 matrix M:

$$M \quad v^{-1} \frac{dQ}{ds} Q^{-1} \tag{11}$$

where Q is a 2×2 matrix. Define a 2×2 matrix P as:

$$P = v^{-1}\frac{dQ}{ds} \tag{12}$$

By substituting equations (11) and (12) into equation (5), the dynamic ray tracing equations in 3-D can be written as

$$\begin{aligned}\frac{dQ}{ds} &= vP \\ \frac{dP}{ds} &= -\frac{1}{v^3}SQ\end{aligned} \tag{13}$$

where $Q_{ij} = \frac{\partial q_i}{\partial \gamma_j}$, $P_{ij} = \frac{\partial P_i}{\partial \gamma_j}$ and γ is ray parameter. S is given as:

$$S = \begin{pmatrix} v_{,11} & v_{,12} \\ v_{,12} & v_{,22} \end{pmatrix}$$

The dynamic ray tracing system has 8 equations for real Q and P, and 16 for complex Q and P in 3-D and is specified in ray centered coordinates (s, q_1, q_2) and ray coordinates (γ_1, γ_2). Červený (1985) has shown that only 8 equations are generally needed for Gaussian beams. The number of equations can be reduced further if only one coordinate system could be used.

The standard dynamic ray tracing system generally will have off-diagonal terms in the matrices Q and P. The existence of these off-diagonal terms is due to the use of two coordinate systems in describing the equations.

2.1.3 Beamwidths

The idea of beamwidth is somewhat nebulous in standard Gaussian beam theory, and a proper mathematical or physical meaning of complex parameters in the Q and P matrices is not considered in routine applications of the method. Complex Q and P can be shown to be a consequence of an approximate solution for complex rays emanating from a source having a small imaginary part to its location in space (Felsen, 1984; Wu, 1985). In practice, beamwidths are defined somewhat arbitrarily and are adjusted to minimize errors in the beam superposition (Klimeš, 1988; Kim and Garmany, 1985) or tuned to minimize errors associated with rapid variations in velocity (Weber, 1988). White et al. (1987) have shown that optimum beamwidths strongly

depend on the specific wave propagation problem and the particular type of boundary interactions occuring in the problem. One of reasons why the concept of optimum beamwidths does not work well is that the total energy of each beam differs for different initial beamwidths. This is true for all of the various optimal beamwidths that have been proposed. If energy flux is to be conserved within a ray tube, then a normalization condition must be applied with respect to the different initial beamwidths. The following section shows how these many of these problems in the standard Gaussian beam method can be remedied by using a dynamic ray tracing system derived from the Hamiltonian of a ray and applying a normalization condition and conservation law of energy flux along a wavefront.

2.2 Vicinity ray tracing system

2.2.1 Derivation

Let us consider the high frequency asymptotic solution to the wave equation in an inhomogeneous medium. In order to obtain the desired approximation, let us assume that the displacement u is expressed in the following form in a generalized coordinate system.

$$w(q_i, \omega) = A(q_i) e^{-i\omega\tau(q_i)} \tag{14}$$

where $i = 1, 2, ...n$ is an n-dimensional configuration space whose coordinates are the n generalized coordinates q_i. A and τ are an amplitude function and a phase function. Both A and τ are functions which can be assumed to be slowly varying with respect to the wavelength λ. The Hamiltonian of a ray is applied in this study to determine the functions A and τ.

Since Fermat's principal of least time can be expressed by the operations of variational calculus, a Lagrangian and Hamiltonian of a seismic ray can be defined similar to those used in describing the mechanics of particles. Fara and Madariaga (1988) , for example, used the Hamiltonian of a seismic ray to develop a perturbation theory to compute the amplitude and travel time of a vicinity ray with respect to a reference ray.

By applying Fermat's principle, the travel time τ from source (s_o) to receiver (s_r) can be written as a path integral over the Langrangian, L, by

$$\tau = \int_{s_o}^{s_r} L(q_i, \dot{q}_i) ds \tag{15}$$

where $\dot{q}_i = \frac{dq_i}{ds}$. The Lagrangian of the ray in generalized coordinates is given by

$$L(q_1, q_2, \dot{q}_1, \dot{q}_2, s) = V^{-1}(\sum_{i=1}^{n} h_i^2 \dot{q}_i^2)^{1/2} \tag{16}$$

where h_i is a scale factor of the i-th unit vector and V is the corresponding velocity. Ray tracing in a general coordinate system (e.g., Cartesian, spherical, and cylindrical) is given by the Euler equation,

$$\frac{d}{ds}(\frac{\partial L}{h_i \partial \dot{q}_i}) = \frac{\partial L}{h_i \partial q_i}, \tag{17}$$

which is derived from the variational principal. The generalized momentum p_i associated with the coordinate q_i is given as follows (Goldstein, 1980, p.339).

$$p_i = \frac{\partial L}{h_i \partial \dot{q}_i} \tag{18}$$

The terms canonical momentum or conjugate momentum are also used for p_i. The Hamiltonian of the ray in the ray centered coordinates can be obtained from the Lagrangian. The Lagrangian of a ray in ray centered coordinates is obtained from equation (16) as

$$L(q_1, q_2, \dot{q}_1, \dot{q}_2, s) = \frac{1}{V}(h^2 + \dot{q}_1^2 + \dot{q}_2^2)^{1/2} \tag{19}$$

where

$$h = h_1 = 1 + \sum_{i=1}^{2} \frac{v_{,i}}{v} q_i \tag{20}$$

and where $\dot{q}_i = \frac{dq_i}{ds}$, $v_{,i} = \frac{\partial v}{\partial q_i}$ and $h_2 = h_3 = 1$. $V = v(s, q_1, q_2)$ is the velocity of a vicinity ray and $v = v(s, 0, 0)$ is the velocity of a central ray. The Lagrangian in equation (19) has s as an independent variable. The conjugate momentum p_i can be expressed, by using equation (18),

$$\begin{aligned} p_1 &= \frac{\partial L}{\partial \dot{q}_1} = \frac{1}{V} \frac{\dot{q}_1}{\sqrt{h^2 + \dot{q}_1^2 + \dot{q}_2^2}} \\ p_2 &= \frac{\partial L}{\partial \dot{q}_2} = \frac{1}{V} \frac{\dot{q}_2}{\sqrt{h^2 + \dot{q}_1^2 + \dot{q}_2^2}}. \end{aligned} \tag{21}$$

Equation (21) can be solved for $\dot{q}_1$ and $\dot{q}_2$, yielding

$$\dot{q}_1 = \frac{hp_1}{V\sqrt{1 - V^2(p_1^2 + p_2^2)}}$$

$$\dot{q}_2 = \frac{hp_2}{V\sqrt{1 - V^2(p_1^2 + p_2^2)}}. \tag{22}$$

The Hamiltonian, H, is expressed as follows:

$$H(q_1, q_2, p_1, p_2, s) = p_1\dot{q}_1 + p_2\dot{q}_2 - L(q_1, q_2, \dot{q}_1, \dot{q}_2, s). \tag{23}$$

By substituting equation (22) into equation (23), the Hamiltonian of a ray in the ray centered coordinates is obtained,

$$H(q_1, q_2, p_1, p_2, s) = -\frac{h}{V}[1 - V^2(p_1^2 + p_2^2)]^{1/2}. \tag{24}$$

The vicinity ray tracing system in the ray centered coordinates can be described in terms of the canonical equations from the Hamiltonian defined in (24). The canonical transform in the ray centered coordinates is obtained from equation (23).

$$\frac{dq_1}{ds} = \frac{\partial H}{\partial p_1} = \frac{h\,V\,p_1}{A}$$

$$\frac{dq_2}{ds} = \frac{\partial H}{\partial p_2} = \frac{h\,V\,p_2}{A} \tag{25}$$

$$\frac{dp_1}{ds} = -\frac{\partial H}{\partial q_1} = \frac{h_{,q_1}}{V}A - \frac{V_{,q_1}\,h}{V^2}A - \frac{h\,V_{,q_1}\,(p_1^2 + p_2^2)}{A}$$

$$\frac{dp_2}{ds} = -\frac{\partial H}{\partial q_2} = \frac{h_{,q_2}}{V}A - \frac{V_{,q_2}\,h}{V^2}A - \frac{h\,V_{,q_2}\,(p_1^2 + p_2^2)}{A} \tag{26}$$

where $A = \sqrt{1 - V^2(p_1^2 + p_2^2)}$. Equations (25) and (26) are comparable to the dynamic ray tracing equations (13), but no paraxial approximations have been made. Červený (1988) has also briefly described the derivation of equations (25) and (26), showing how they become the standard dynamic ray tracing equations if paraxial approximations are substituted for h and V.

To simplify equations (25) and (26), let us define η as the angle difference between the tangential vectors of a central ray and a vicinity ray in the $(\hat{t}, \hat{e}_1)$

plane and ζ as the angle difference between the tangential vectors of a central ray and of a vicinity ray in the $(\hat{t}, \hat{e}_2)$ plane in the ray centered coordinates (figure 2). q_i is the distance from the central ray to the the vicinity ray along the $\hat{e}_i$. From figure 3 it is seen that the curvature (K_i) of the wavefront is a function of $tan\ \eta_i$ and q_i,

$$K_i = \frac{tan\ \eta_i}{q_i} = \frac{1}{R_i} \tag{27}$$

where $i = 1, 2$ and R_i is the radius of curvature of the wavefront. Using the definition of η from figures 2 and 3, equation (25) can be rewritten as

$$\frac{dq_1}{ds} = h\ tan\ \eta$$

$$\frac{dq_2}{ds} = h\ tan\ \zeta \tag{28}$$

Using equations (21) and (28), p_i can be expressed with respect to $tan\ \eta$ and $tan\ \zeta$.

$$p_1 = \frac{tan\ \eta}{VB}$$

$$p_2 = \frac{tan\ \zeta}{VB} \tag{29}$$

where $B = \sqrt{1 + tan^2\eta + tan^2\zeta}$
Differentiating equation (29) with respect to s yields

$$\frac{dp_1}{ds} = \frac{sec^2\eta}{VB^3}(1 + tan^2\zeta)\frac{d\eta}{ds} - \frac{V_{,s}\ tan\ \eta}{V^2B} - \frac{tan\ \eta\ tan\ \zeta\ sec^2\zeta}{VB^3}\frac{d\zeta}{ds}$$

$$\frac{dp_2}{ds} = \frac{sec^2\zeta}{VB^3}(1 + tan^2\eta)\frac{d\zeta}{ds} - \frac{V_{,s}\ tan\ \zeta}{V^2B} - \frac{tan\ \eta\ tan\ \zeta\ sec^2\eta}{VB^3}\frac{d\eta}{ds} \tag{30}$$

The quantity A can be rewritten using expressions for p_i given in (29):

$$A = \sqrt{1 - V^2(p_1^2 + p_2^2)} = \sqrt{1 - \frac{tan^2\eta + tan^2\zeta}{B^2}} = \frac{1}{B}$$

η and ζ are located within $\hat{t}$ $\hat{e}_1$ plane and within $\hat{t}$ $\hat{e}_2$ plane respectively, and both planes are orthogonal to each other. This orthogonality simplifies the derivation of vicinity ray tracing system. $\frac{d\eta}{ds}$ and $\frac{d\zeta}{ds}$ can be obtained by

equating equations (26) and (30). Finally, the vicinity ray tracing system in the ray centered coordinates can be given as

$$\frac{dq_1}{ds} = h \tan \eta$$

$$\frac{dq_2}{ds} = h \tan \zeta \tag{31}$$

$$\frac{d\eta}{ds} = \cos^2\eta\left(\frac{V_{,s}}{V} B^2 \tan \eta + \frac{C}{\cos^2\eta} + D \tan \eta \tan \zeta\right)$$

$$\frac{d\zeta}{ds} = \cos^2\zeta\left(\frac{V_{,s}}{V} B^2 \tan \zeta + \frac{D}{\cos^2\zeta} + C \tan \eta \tan \zeta\right) \tag{32}$$

where

$$C = h_{,q_1} - \frac{V_{,q_1} h}{V} B^2$$

$$D = h_{,q_2} - \frac{V_{,q_2} h}{V} B^2$$

Note that C and D and the equations for η and ζ depend on the velocity of the medium along the vicinity ray, $V(s,0,q_2)$ or $V(s,0,q_1)$ rather than on the velocity of the medium along the central ray, $V(s,0,0) = v(s)$. For a velocity model specified in Cartesian coordinates, the velocity V and its derivatives $V_{,q_i}$ can be calculated by transforming the positions of the vicinity ray in ray centered coordinates $(0,q_1,0)$ and $(0,0,q_2)$ to Cartesian coordinates.

C and D can be expanded at $q_i = 0$, by using equations (7), (8) and (29).

$$C \approx -\frac{v_{,q_1 q_1}}{v} q_1 - \frac{v_{,q_1} + v_{,q_1 q_1} q_1}{v}(\tan^2\eta + \tan^2\zeta)$$

$$D \approx -\frac{v_{,q_2 q_2}}{v} q_2 - \frac{v_{,q_2} + v_{,q_2 q_2} q_2}{v}(\tan^2\eta + \tan^2\zeta) \tag{33}$$

There is no advantage, however, in making such an expansion. The accuracy of this expansion decreases as the distances q increase, and it requires the calculation of the second spatial derivative of velocity.

Since the vicinity ray tracing system calculates q_i and η_i values by using V and $V_{,q_i}$ it is not necessary to employ the method of matching paraxial phase (Červený and Hron, 1980) to determine new initial conditions on q_i and η_i when vicinity rays are transmitted through or reflected by discontinuities. Since second spatial derivatives of velocity are not used in the vicinity

ray tracing system, no jumps q_i or η_i are induced by velocity gradient discontinuities. At first order discontinuities in velocity, new initial conditions on q_i and η_i are computed by simply applying Snell's law to both the central ray and the vicinity ray.

2.2.2 Initial conditions

The initial conditions of the vicinity ray tracing system at the source point depend on the type of source. For a point source the initial conditions are

$$q_i|_{s=0} = 0$$
$$\eta_i|_{s=0} = \eta_i^I \tag{34}$$

and for a line source they are

$$q_i|_{s=0} = q_i^I$$
$$\eta_i|_{s=0} = \eta_i^I \tag{35}$$

where superscript I denotes the initial value of the parameter. The initial condition on q_i^I in the case of a line source depends on the intensity or shape of the source. q_i^I will be the half length of the line source.

When the wavefield is computed by a superposition of Gaussian beams, the initial value chosen for η_i^I will depend on the density of beams in the superposition. Beamwidths are taken to be roughly equal to the Fresnel volume surrounding the central ray. The Fresnel volume is estimated from the frequency and the separation of the vicinity rays from the central ray. To achieve an accurate estimate of the Fresnel volume, the spacing of vicinity rays is taken to overlap the spacing of central rays. In the synthetic seismograms shown in a later section, the frequency band and spacing of vicinity rays is such that the paraxial Fresnel volume is located between the central ray and the vicinity ray except near the x-caustic and y-caustics as defined in Chapman and Drummond (1982). In the vicinity ray tracing system, the x-caustic corresponds to $q_i = 0$ and the y-caustic $\eta_i = 0$.

The physical meaning of q_i is the distance from the central ray to the vicinity ray, and is determined fully from equations (31) and (32). The variation of q_i describes the change in amplitude, and the variation of η_i describes the geometry of the wavefront. These properties of q_i and η_i can be

applied to many related problems such as two point ray tracing, calculation of the travel time of a vicinity ray, amplitude inversion, and correction of q_i and p_i at a discontinuity. The vicinity ray tracing system in equations (31) and (32) is obtained without using any paraxial approximations. Thus, the system should give more accurate predictions of the wavefield in the neighborhood of a central ray when the medium has strong velocity gradients.

As shown in equations (31) and (32), the vicinity ray tracing system is described by 4 equations in 3-D; by contrast, the standard dynamic ray tracing system requires 8 equations. The reason that the vicinity ray tracing system requires fewer equations is that only ray centered coordinates are used instead of a combination of ray centered coordinates and ray coordinates.

2.2.3 Computation of travel time near a central ray

The computation of the travel time to a receiver near a central ray is just as simple in the vicinity ray tracing system as in the standard method of dynamic ray tracing using the paraxial approximation. Figure 3 illustrates the calculation of the travel time, $\tau(s, n_1, n_2)$ at point N(s,n_1, n_2). The determination of s and n_i for a specified point N in ray centered coordinates is important to obtaining accurate estimates of travel time and amplitude of the vicinity ray with respect to a central ray. The rough approximations contained in the standard paraxial technique may produce spurious oscillations in the superposition of Gaussian beams (e.g., Madariaga, 1984) and break down if the central ray is far from the receiver.

Here, we describe an improved method for the determination of a specified point in ray centered coordinates. We begin by writing travel time field, $\tau(s, n_1, n_2)$ of the specified point (e.g., receiver), N in the ray centered coordinates as

$$\tau(s, n_1, n_2) = \tau(s) + \sum_{i=1}^{2} \epsilon_i \, \Delta\tau_i \tag{36}$$

where

$$\epsilon_i = 1 \quad for \quad q_{n_i} \times \eta_i > 0 : convex \; wave \; front.$$
$$\epsilon_i = 0 \quad for \quad q_{n_i} \times \eta_i \quad 0 : planar \; wave \; front.$$
$$\epsilon_i = 1 \; for \; q_{n_i} \times \eta_i < 0 : concave \; wave \; front.$$

ϵ_i corresponds to the sign of M in the standard dynamic ray tracing system along the $\hat{e}_i$ (Červený and Pšencík, 1983). $\Delta\tau_i$ is the travel time difference

along the $\hat{\epsilon}_i$ direction between the points N and S (figure 3). The travel time difference $\Delta\tau(s, q_{n_1}, q_{n_2})$ between S and N, is obtained from

$$\Delta\tau_i = \frac{\Delta n_i}{v(s)} \tag{37}$$

where Δn_i is the distance between C and N. The distance Δn_i is simply calculated as shown in figure 3, and is given by

$$\Delta n_i = \sqrt{R_i^2 + n_i^2} \quad R_i \tag{38}$$

where R_i is the radius of curvature of the wavefront, which is perpendicular to $\hat{e}_i$. $\Delta\tau_i$ is obtained by substituting equation (38) into (37),

$$\Delta\tau_i = \frac{\Delta n_i}{v(s)} = \frac{\sqrt{R_i^2 + n_i^2} \quad R_i}{v(s)} \tag{39}$$

To facilitate comparison with the standard Gaussian beam method, equation (39) can be expanded; for $\frac{n_i}{R_i} \ll 1$,

$$\Delta\tau_i = \frac{R_i}{v}\left(\sqrt{1 + \frac{n_i^2}{R_i^2}} - 1\right) \approx \frac{n_i^2}{2v\ R_i} \tag{40}$$

The factor $\frac{1}{vR_i}$ in equation (40) corresponds to real M in the expression for the standard Gaussian beam method, where n_i is small. The travel time $\tau(s, n_1, n_2)$ can be rewritten by substituting equation (39) into (36),

$$\tau(s, n_1, n_2) = \tau(s) + \sum_{i=1}^{2} \epsilon_i \frac{\sqrt{R_i^2 + n_i^2} - R_i}{v(s)} \tag{41}$$

Note in equation (41) that the travel time of a specified point (s, n_1, n_2) is obtained without using any paraxial approximations. The travel time of a specified point $\tau(s, n_1, n_2)$ is easily and accurately calculated with respect to the travel time of central ray $\tau(s)$ since the radius of curvature of the wavefront, R_i, is a function of q_i and η_i.

Let $q\prime_i$ denote the normal distance to the central ray from point B, where B is the intersection of the wavefront of the central ray and vicinity ray

(figure 3). The curvature (K_i) and the radius of curvature of the wavefront (R_i) can be expressed as follows (Červený, 1981).

$$R_i = \frac{1}{K_i} = \frac{qt_i}{vp_i} \tag{42}$$

Substituting equation (29) into (42) produces,

$$R_i = \frac{qt_i}{vp_i} = \frac{qt_i}{\sin \eta_i} = \frac{qt_i}{\sin \eta_i} = \frac{q_i}{\tan \eta_i} \tag{43}$$

Let $\tilde{q}_i$ denote the distance from S to B along the wavefront. The wavefront coordinates $(s, \tilde{q}_1, \tilde{q}_2)$ are defined from projections of the unit vectors $\hat{f}_i$ to the plane normal to the central ray that become the unit vectors of the ray centered coordinates $\hat{e}_1$ and $\hat{e}_2$ (figure 3). The relation between q_i anf $\tilde{q}_i$ can be represented using R_i:

$$R_i - \frac{q_i}{\tan \eta_i} = \frac{\tilde{q}_i}{\eta_i} \tag{44}$$

Equation (44) determines the Jacobian J between the ray centered coordinates and the wavefront coordinates:

$$q_1 q_2 = J \tilde{q}_1 \tilde{q}_2 \tag{45}$$

where $J = \frac{\eta_1 \eta_2}{\tan \eta_1 \tan \eta_2}$. Equation (44) shows that the curvature of a wavefront K_i or the radius of curvature of the wavefront R_i can be written as a simple function of q_i and η_i. When $n_i = q_i$, equation (39) can be rewritten by using equation (44),

$$\Delta\tau_i = \frac{q_i}{v(s)\tan \eta_i}(\sqrt{1 + \tan^2\eta_i} - 1) \tag{46}$$

By substituting equation (46) into (36), the travel time of the vicinity ray $\tau(s, q_1, q_2)$ can be expressed as:

$$\tau(s, q_i) = \tau(s) + \sum_{i=1}^{2} \epsilon_i \frac{q_i}{v(s)\tan \eta_i}(\sqrt{1 + \tan^2\eta_i} - 1) \tag{47}$$

Equation (47) shows that $\Delta\tau$ also can be calculated by just using q_i and η_i without calculating K_i or R_i.

$\tau(s, n_i)$ and $\tau(s, q_i)$ in equations (41) and (47) can be described in terms of a known point $s = s_o$ along the central ray. The quantity $\tau(s)$ can be

can be expanded with respect to $\tau(s_o)$ by using a Taylor expansion about s_o. Terms higher than second order are negligible and will be neglected.

$$\tau(s) \approx \tau(s_o) + \frac{\partial \tau(s)}{\partial s}\Big|_{s=s_o}(s - s_o) + \frac{1}{2}\frac{\partial^2 \tau(s)}{\partial s^2}\Big|_{s=s_o}(s - s_o)^2 + \ldots \qquad (48)$$

It is easy to see that

$$\frac{\partial \tau(s)}{\partial s}\Big|_{s=s_o} = \frac{1}{v(s_o)}$$

and that

$$\frac{\partial^2 \tau(s)}{\partial s^2}\Big|_{s=s_o} = \frac{v_{,s}(s_o)}{v^2(s_o)} \qquad (49)$$

The travel time of the central ray $\tau(s)$ can be rewritten by substituting equation (49) into (48).

$$\tau(s) = \tau(s_o) + \frac{1}{v(s_o)}(s - s_o) - \frac{1}{2}\frac{v_{,s}(s_o)}{v^2(s_o)}(s - s_o)^2 \qquad (50)$$

Combining the expressions (41), (47), and (50), the travel time $\tau(s, n_i)$ and $\tau(s, q_i)$ is approximated by

$$\begin{aligned}
\tau(s, n_i) &= \tau(s_o) + \frac{1}{v(s_o)}(s - s_o) - \frac{1}{2}\frac{v_{,s}(s_o)}{v^2(s_o)}(s - s_o)^2 \\
&\quad + \sum_{i=1}^{2} \frac{\epsilon_i(\sqrt{R_i^2 + n_i^2} - R_i)}{v(s)} \\
\tau(s, q_i) &= \tau(s_o) + \frac{1}{v(s_o)}(s - s_o) - \frac{1}{2}\frac{v_{,s}(s_o)}{v^2(s_o)}(s - s_o)^2 \\
&\quad + \sum_{i=1}^{2} \frac{\epsilon_i q_i}{v(s)\tan\eta_i}(\sqrt{1 + \tan^2\eta_i} - 1)
\end{aligned} \qquad (51)$$

$\tau(s, q_i)$ denotes the travel time of the vicinity ray, and q_i is calculated by equations (31) and (32), while $\tau(s, n_i)$ indicates the travel time of a specified point N, such as a receiver point, in the ray centered coordinates. Note that although a Taylor expansion has been used, it is a Taylor expansion along the direction of the central ray rather than along a direction perpendicular to the central ray. The standard Gaussian beam and paraxial ray methods make a Taylor expansion of travel time in the direction perpendicular to the central ray as well. In equation (51) it is usually possible to select $s_o = s$, *avoiding the Taylor expansion along the central ray.*

2.2.4 Fresnel beamwidths

The beamwidth F_i is defined as the distance from the central ray to the paraxial Fresnel volume along the $\hat{e}_i$ direction. The Fresnel volume encloses all virtual rays in the neighborhood of the central ray such that the travel time of any virtual ray differs from the travel time of the central ray by one-half period (Stone, 1963; Kravtsov and Orlov, 1980; Marcuse, 1982; Červený, 1988). Given a frequency, the Fresnel volume is estimated from the locus of a vicinity ray and a central ray. The travel time difference between the central ray and the paraxial Fresnel volume is given as

$$\begin{aligned} \tau(s, F_1, 0) - \tau(s, 0, 0) &= \gamma \\ \tau(s, 0, F_2) - \tau(s, 0, 0) &= \gamma \end{aligned} \tag{52}$$

where γ is the half period. Equation (52) states that a point on the Fresnel volume $(s, F_1, 0)$ or $(s, 0, F_2)$ has a half period time difference with respect to the wavefront that passes through the point $(s, 0, 0)$ on the central ray. Formulae for the beamwidths F_i are then obtained by substituting (51) and (44) into (52),

$$\begin{aligned} F_1 &= \sqrt{\gamma^2 V_1^2 + 2\gamma V_1 \frac{q_1}{tan(\eta_1)}} = \sqrt{\gamma^2 V_1^2 + 2\gamma V_1 R_1} \\ F_2 &= \sqrt{\gamma^2 V_2^2 + 2\gamma V_2 \frac{q_2}{tan(\eta_2)}} = \sqrt{\gamma^2 V_2^2 + 2\gamma V_2 R_2} \end{aligned} \tag{53}$$

For high frequency (small γ), the beamwidth given by (53) is approximately proportional to $\sqrt{2\gamma R_i V_i} = \sqrt{\frac{R_i V_i}{f}}$. Equation (53) is the same as the classical definition of Fresnel's half period zones (e.g., Jenkin's and White, 1937).

2.3 The synthesis of seismograms

The zeroth order high frequency asymptotic solution to the wave equation in generalized coordinates was given in equation (14). Let us consider a point N, located close to the central ray, specified by the ray centered coordinates, (s, n_1, n_2), that is, $S = (s, n_1, n_2)$. The zeroth order asymptotic solution to the reduced wave equation in the ray centered coordinates can be expressed in the form

$$g(S, \omega) = A(S) e^{-i\omega\tau(S)} (-i)^k sgn(\omega) \tag{54}$$

The amplitude function A is real and can be determined by applying the conservation of energy flux and a normalization condition (Beiser, 1969, p. 156; Gasiorowicz, 1974, p. 45). τ is the travel time of the central ray. k is the value of the KMAH index whose value is increased by one whenever the sign of q_i changes along the ray. The KMAH index represents the $\frac{\pi}{2}$ phase shift whenever the ray touches a caustic surface (Chapman and Drummond, 1982).

2.3.1 Source-time functions

For a source-time function $f(t)$ specified as the real part of an analytic function $y(t)$, the wave field is given by evaluating a convolution:

$$u(S,t) = Re[g(S,t) * y(t)] \tag{55}$$

Rewriting equation (55) as

$$u(S,t) = \frac{Re}{\pi} \int_{-\infty}^{\infty} g(S,\omega) y(\omega)\, e^{-i\omega t}\, d\omega \tag{56}$$

and substituting equation (54) for $g(S,\omega)$ gives

$$u(S,t) = \frac{A(S)}{\pi} Re \int_{-\infty}^{\infty} (-i)^k\, sgn(\omega) y(\omega) e^{-i\omega(t-\tau)} d\omega - \frac{A(S)}{\pi} Re[y(t-\tau)(-i)^k] \tag{57}$$

$y(t)$ is the analytic time series represented by

$$y(t) = f(t) - ih(t) \tag{58}$$

where $f(t)$ and $h(t)$ are Hilbert transform pairs (Bracewell, 1978). The analytic function corresponding to any realistic source-time function can be constructed by choosing $y(t)$ to be a generalized delta function and convolving that function with $y(t)$. Some possible forms for $y(t)$ are

1. a delta function (Chapman,1977; Chapman and Drummond, 1982)

$$y(t) = \delta(t) - i\frac{1}{\pi t} \tag{59}$$

2. a Gaussian wavelet

$$y(t) \approx \frac{1}{\pi\gamma} e^{-(\frac{t}{\gamma})^2} e^{-i\pi t} \tag{60}$$

3. or a resonance function (Madariaga and Papadimitriou, 1985)

$$y(t) = \frac{1}{\pi}\left[\frac{\Delta t}{t^2 + (\Delta t)^2} - i\frac{t}{t^2 + (\Delta t)^2}\right] \tag{61}$$

γ is the prevailing frequency of the Gaussian wavelet and Δ is the sampling interval or the half period for the discrete time series $y(t)$.

The Gaussian wavelet (60) is useful for simulating a narrow band source, while (61) is useful for simulating broad band responses. Equations (59), (60) and (61) can be constructed to be a generalized delta function by requiring

$$\int_{-\infty}^{\infty} Re\ y(t)dt = 1 \tag{62}$$

2.3.2 Beamwidths

For a point source, it is natural to assume that the amplitude distribution within a beam is Gaussian. The amplitude function A at a specified point N will be described as a generalized Gaussian function of the form

$$A(S) \quad C exp[\ -(\frac{n_1}{F_1})^2 \quad -(\frac{n_2}{F_2})^2] \tag{63}$$

where F_i are the half-widths of the paraxial volume. With this amplitude distribution, the energy (probability of finding a ray) along the the paraxial Fresnel volume of half-width F_i is proportional to $\frac{1}{e^2}$ and its amplitude is proportional to $\frac{1}{e}$ with respect to the central ray. If the expression for the amplitude function is viewed as a generalized delta function, C can be chosen from a normalization condition in space and time. Generally, F_i is chosen to be equal to the half-width of the paraxial volume as defined in equation (53). We assume that the contribution of a beam to the receiver is zero when the distance between the ray and receiver is larger than q_i. Without loss of generality, this condition eliminates a singularity near both x and y caustics. Near the x and y caustic, the half-width of the paraxial Fresnel volume F_i may become larger than q_i. In the these regions the beamwidth is taken to be equal to q_i rather than F_i and its amplitude distribution will be a generalized rectangular function instead of a generalized Gaussian function. These modifications near x and y caustics do not violate energy conservation and the normalization condition.

2.3.3 Energy conservation and normalization of beams

Using equations (54) and (57) the complex displacement u of a beam specified at a point N in the ray centered coordinates is

$$u(S,t) = C exp[-(\frac{n_1}{F_1})^2 - (\frac{n_2}{F_2})^2] (-i)^k \, y(t - \tau), \qquad (64)$$

where amplitude factor C is obtained by using the law of conservation of energy flux and a normalization condition. This approach for determining C differs from the approach followed in the standard Gaussian beam technique, where C is obtained by evaluating the superposition integral by stationary phase and requiring the result to reproduce ray theory in regions where it is valid. In contrast to the standard Gaussian beam method, beams are interpreted as the probability of finding a ray at a given point and time. This probability distribution is assumed to be a Gaussian distribution whose unit area is always 1 with respect to n_i and t. This constraint guarantees that the energy of a beam (ray tube) is conserved with respect to the space and time, and that the determinant of the propagator matrix in dynamic ray tracing system is constant along the ray (Liouville's theorem) (Červený and Pšenčík, 1983; Kim, 1985; Klimeš, 1988). The wave function u(S,t) then describes the probability of finding a ray with a statistical state, which is characterized by u. Because the total energy in a beam is conserved along the wavefront, it is necessary to transform from the ray centered coordinates to the wavefront coordinates. The Jacobian between the ray centered and the wavefront coordinates is given in equation (45). The conservation law of energy flux and the normalization condition imply that the probability (P) of finding a ray within a given space is

$$P(S,t) = < u \mid u >_{s,0,0} = \int\int_{-\infty}^{\infty} dq_1 \, dq_2 \, J \, u^*(S,t) \qquad (65)$$

where the symbol * denotes the complex conjugate. The constant C in equation (64) is determined by solving equation (65) and by considering the normalization factor D for a radiation pattern at the source. The integral of equation (65) yields

$$P(S,t) = C^2 \frac{F_1 F_2 \pi}{2} \frac{J}{D^2} \qquad (66)$$

The constant D depends on the take-off angle δ and azimuth ϕ (Aki and Richards, 1980, p. 82; Klimeš, 1984b). The constant C is then obtained as

$$C = \frac{\sqrt{2}D}{\sqrt{J\ \pi\ F_1 F_2}}$$

A(S) can be rewritten as follows by substituting expression for C into (63)

$$A(S) = \frac{\sqrt{2}D}{\sqrt{J\ \pi\ F_1 F_2}} exp[-(\frac{n_1}{F_1})^2 - (\frac{n_2}{F_2})^2] \qquad (67)$$

The calculation of the travel time $\tau(s, n_i)$ in (54) is given in equations (51). The final wavefield of a ray at a specified point is is then obtained as

$$u(S,t) = \frac{\sqrt{2}D}{\sqrt{J\ \pi^3 F_1 F_2}} exp[\ (\frac{n_1}{F_1})^2 + (\frac{n_2}{F_2})^2] y(t - tau)\ (-i)^k \qquad (68)$$

Equation (68) can be modified to represent source-time functions such as a generalized rectangle function or combination of generalized functions for a line source. The representation of a line source depends on its intensity distribution with length. Generally, the expression for a line source is more complicated than that for a point source.

The form of equation (68) can be shown to be quite similar to the expression for a standard Gaussian beam when paraxial approximations are substituted for phase and the expression of the half-width of the paraxial volume is substituted for F_i. The approach and concepts used in deriving the vicinity ray tracing system, however, are quite different from those used in the standard Gaussian beam method. The number of equations required in this method is 9, by contrast to 21 in the standard Gaussian beam method. This method uses exact positions of vicinity rays while the standard Gaussian beam method uses estimated values based on a Taylor expansion about the central ray. Beamwidth in this method is the distance from the central ray to the paraxial Fresnel volume and is fully determined by equation (53), while beamwidth in the standard Gaussian beam method is usually chosen arbitrarily and not given any physical meaning.

2.3.4 Superposition of beams

For the wavefield obtained by superposition of all beams we shall use upper-case U, instead of lower-case u, which is reserved for an individual beam.

Note that the wavefield u corresponding to an individual beam is a function of vertical take-off angle and azimuth (δ and ϕ), which specify the central ray under consideration. Thus we shall write u(S, t, δ, ϕ) instead of u(S,t). The wavefield U(S,t) will be described by superposition of individual beams (rays) with respect to δ and ϕ.

$$U(S,t) = \int_{\delta_o}^{\delta} \int_{\phi_o}^{\phi} u(S,t,\delta,\phi) d\delta d\phi \tag{69}$$

When the integrand of equation (69) is sufficiently smooth for a given S and t, it can be discretized as

$$U(S,t) = \sum_{j=0}^{N} \sum_{k=0}^{M} u(S,t,\delta_j,\phi_k) \Delta\delta_j \Delta_k \tag{70}$$

where the quantities $\Delta\delta_j$ and $\Delta\phi_k$ are determined from a given system δ_j and ϕ_k (Červený, 1983b). The wavefield is calculated in (69) or (70) by summing up each ray's contribution at a specified point, its wavelet having a Gaussian distribution both in space and time. As in the Gaussian beam method (Červený, 1983), this method also does not require two-point ray tracing to compute the seismic wavefield.

Since the energy of a beam is conserved along the wavefront, $U(s,t)$ in equation (69) can be rewritten in the wavefront coordinates by using the Jacobians in equation (45)

$$U(S,t) = \int_{\delta_o}^{\delta} \int_{\phi_o}^{\phi} \frac{\sqrt{2}D}{\sqrt{J\ \pi^3 F_1 F_2}} exp[-(\frac{\tilde{n}_1}{J_1 F_1})^2 \quad (\frac{\tilde{n}_2}{J_2 F_2})^2] \ y(T) \ (\ \ i)^k d\delta d\phi \tag{71}$$

As a shown in equations (45) and (45), the Jacobians J_1 and J_2 between the ray centered and the wavefront coordinates give

$$J_i n_i \quad \tilde{n}_i$$

$$\tilde{n}_i \quad R_i \alpha_i \tag{72}$$

where R_i is the radius of wavefront curvature.

2.3.5 Superposition in a homogeneous medium

It is easy demonstrate that the superposition integral returns simple ray theory in a homogeneous medium. In a homogeneous medium, $U(S,t)$ is represented simply because $R_1 = R_2 = S$, and S is the total distance from the source to the receiver. The parameters in a homogeneous medium are given as:

$$R_2 = S \qquad R_2 = S$$

$$\alpha = c_1 + \delta$$

$$\beta = c_2 + \phi \tag{73}$$

and

$$d\alpha = d\delta$$

$$d\beta = d\phi \tag{74}$$

where c_1 and c_2 are constant. Substituting equations (72),(73),and (74) into (71), then gives

$$U(S,t) = \frac{\sqrt{2}D}{\sqrt{\pi^3 J F_1 F_2}} \int_{\delta_o}^{\delta} \int_{\phi_o}^{\phi} exp[-(\frac{R_1\alpha}{J_1 F_1})^2 - (\frac{R_2\beta}{J_2 F_2})^2]\, y(T)\,(-i)^k\, d\alpha d\beta$$

$$= \frac{\sqrt{2}D}{S\sqrt{\pi}}\, y(T)\,(-i)^k \tag{75}$$

where $J = J_1 J_2$

Equation (75) shows that the displacement of $U(s,t)$ in a homogeneous medium is proportional to $\frac{1}{S}$, the distance between source and receiver. Note that the superposition is independent of the choices made for the initial conditions for the spacing of vicinity rays.

3 Numerical Example

A numerical example was chosen to test the superposition of Gaussian beams defined from the vicinity ray tracing system. The model was not designed to be geophysically realistic, but rather to illustrate the theoretical phenomena near the caustic. The velocity of the medium is given by

$$v(z) \quad 2.5 + 0.1 \times z \quad for \quad z \leq 10 \ Km$$

$$v(z) = 3.5 + 0.4 \times (z \quad 10) \quad for \quad z > 10 \ Km$$

The model has a discontinuity in the first derivative of velocity at z= 10 Km but velocity itself remains continuous (figure 4). In the vicinity ray tracing system, no phase matching method is required at a discontinuity of the first derivative of velocity. Figure 5 shows the results of ray tracing ,showing a triplication in the range 32.4 to 48.3 Km from the source. Two caustics are located at $x \approx$32.4 Km and $x \approx$46.3 Km.

Figure 6 shows the vertical component synthetic seismograms computed by superposing Gaussian beams defined from vicinity rays, called "VRT seismograms." To calculate these seismograms, 64 rays are used with a 1° increment of take-off angle. The source is assumed to be an explosive point source, and the initial conditions are $\eta_o = 5$ degrees and $q_o \quad 0$. A monochromatic pulse of frequency 5 Hz is used. The beamwidths are defined by equation (53) using the definition of the Fresnel volume. WKBJ synthetic seismograms are computed for comparison with the VRT seismograms (figure 7). As shown in figures 7 and 8, the two methods closely agree with one another. Amplitude differences between two methods are less than 5 %. Diffractions are shown near the caustics in both methods. The diffraction near the caustic at $x \approx$32.4 Km decays faster than near the caustic at $x \approx$46.4 Km because the beamwidth (Fresnel volume) varies more slowly at the former than at the latter. Some differences in the frequency content of the diffraction from the caustic at $x \approx$32.4 km can be seen. These differences were generated by allowing for a broad frequency spectrum in the WKBJ method by using a delta function source and then convolving the result with a narrow band source pulse. The superposition of vicinity rays, on the other hand, is such that only the frequencies contained in the narrow band source pulse can be seen. This is because the half-width of the paraxial Fresnel volume (beamwidth) was computed only for the center frequency of the narrow band source pulse.

4 Conclusions

Because paraxial approximations are made, the standard dynamic ray tracing system works in only a limited region near the central ray at distances less than the scale length of the medium. Its use of two coordinate systems results in a an increased number of equations needed to describe the dynamic properties of a wavefront. An improved system of dynamic ray tracing equations can be developed from the Hamiltonian of a ray and its canonical equations. This improved system, which we have called the vicinity ray tracing equations, is specified by only 4 equations in addition to the kinematic ray tracing equations. By contrast, the standard dynamic ray tracing equations based on paraxial approximations require 8 equations and their associated Gaussian beams require 16 equations. Unlike the standard dynamic ray tracing system, the vicinity ray tracing system does not require the evaluation of second spatial derivatives of velocity along a ray. The vicinity ray tracing equations will thus have advantages in accuracy and in computer time over standard dynamic ray tracing. Since only first spatial derivatives of velocity are used in the vicinity ray tracing system, no phase matching is required at discontinuities in velocity gradient. At velocity discontinuities, new initial conditions on the vicinity rays are determined by applying Snell's Law to the vicinity rays.

By applying conservation of energy flux and a normalization condition, an improved Gaussian beam technique can be developed by superposing vicinity rays. In this superposition, beamwidths are set equal to the half-width of the paraxial Fresnel volume. An example calculation demonstrates that this definition of beamwidth can approximate diffraction effects.

REFERENCES

Aki, K., and Richards, P. G., 1980. Quantitative seismology: Theory and methods, vol. I, W. H. Freeman and Co.

Babič, V. M., 1979. The boundary-layer method in diffraction problems, Springer-Verlag, pp.60-78.

Bracewell, A., 1978. The Fourier transform and its applicatons, McGraw-Hill, p. 69-95.

Červený, V., and Hron, F., 1980. The ray series method and dynamic ray tracing system for three-dimensional inhomogeneous media, Bull. Seism. Soc. Am., 70, 47-77.

Červený, V., 1981. Dynamic ray tracing across curved interfaces, Stanford Exploration Project, No. 28, 61-74. Dept. of Geophysics, Stanford Univ.

Červený, V., Popov, M. M., and Pšenčík, I., 1982. Computation of wave fields in inhomogeneous media-Gaussian beam approach, Geophys. J. R. astr. Soc., 70, 119-128.

Červený V., and Pšenčík, I., 1983. Gaussian beams and paraxial ray approximations in three-dimensional elastic inhomogeneous media, J. Geophys., 53, 1-15.

Červený V., 1983. Synthetic body wave seismograms for laterally varying layered structure by the Gaussian beam method, Geophys. J. R. astr. Soc., 73, 389-426.

Červený, V., 1985. The application of ray tracing to numerical modeling of seismic wave fields in complex structure, Handbook of Geophysical Exploration, Section I, Vol. 15A, 29-37.

Červený, V., 1988. Ray methods for three-dimensional seismic modeling, lecture notes, Inst. of Geophys. Charles Univ., Prague, ch. 6, p. 82-109.

Chapman, C. H., 1978. A new method for computing Synthetic seismograms, Geophys. J. R. astr. Soc., 54, 481-513.

Chapman, C. H., and Drummond R., 1982. Body-wave seismograms in inhomogeneous media using Maslov asymptotic theory, Bull. Seism. Soc. Am., 72, S227-S317.

Farra V., and Madariaga, R., 1987. Seismic waveform modeling in heterogeneous media by ray perturbation theory, J. Geophys. Res. 92, 2697-2712.

Goldstein, H., 1980. Classical Mechanics, Addison-Wesley Publ. Co. p. 339-498

Jenkins, A. F., and White, H. ed., 1937. Fundamentals of physical optics, McGraw-Hill Book Co., p. 146-201.

Kravtsov, Y. I., and Orlov, Y. I., 1980. Limits of applicability of the method of geometric optics and related problems, Sov. Phys. Usp., 23, 475-496 (English translation by M. V. King, Am Inst. Phys., 1981)

Kim, W., 1986. Gaussian beam synthetic body-wave seismograms using *IPGT method with optimum beamwidths*, *M.S. thesis*, *The Univ. of* Texas at Austin.

Kim, W., and Garmany, J., 1985. Optimum beamwidths for Gaussian beams in three dimensions, E.O.S., 66, 980 (Abstract, Fall 1985 A.G.U. meeting)

Klimeš, L., 1984. The relation between Gaussian beams and Maslov asymtotic theory, Studia Geophys. and Geod., 28, 237-247.

Klimeš, L., 1988. Optimization of the shape of Gaussian beam of a fixed length, Geophys. J. R. astr. Soc., in press

Madariaga, R., 1984. Gaussian beam synthetic seismograms in a vertically varying medium, Geophys. J. R. astr. Soc., 79, 589-612.

Madariaga, R., and Papadimitriou, p., 1985. Gaussian beam modeling of upper mantle phases, Annales Geophys., 3, 6, 799-812.

Marcuse, D., 1982, Light Transmissions Optics, Van Nostrand Reinhold Co., p. 94-124.

Popov, M. M., and Pšenčik, I., 1978. Computation of ray amplitudes in inhomogeneous media with curved interfaces, Studia et geod., 22, 248-258.

Popov, M. M., 1982. A new method for computation of wavefields using Gaussian beams, Wave Motion, 4, 85-97.

Stone, J. M, 1963. Radiation and optics, McGraw-Hill Book Co., p. 115-209.

Weber, M., 1988. Application of the Gaussian beam in refraction seismology-Urach revisited, Geophys. J., 92, 365-377

White, B. S., Norris, A., Bayliss, A. and Burridge, R., 1987. Some remark on the Gaussian beam summation method, Geophys. J. R. astr. Soc., 89, 579-636.

Wu, R.-S., 1985. Gaussian beams, complex rays, and the analytic function in smoothly inhomogeneous media, Geophys. J. R. astr. Soc., 83, 93-110

Figure Captions

Figure 1

The ray centered coordinates (s, q_1, q_2): $\hat{t}$ is the unit tangent vector of a central ray and $\hat{e}_1$ and $\hat{e}_2$ are the unit normal vectors to $\hat{t}$. The coordinate s measures the arclength along a central ray from an arbitrary reference point. q_1 and q_2 represent length coordinates and form a two dimensional orthogonal coordinate system in the plane normal to Ω at O.

Figure 2

The geometry of the vicinity ray tracing system: η_i is the angle difference between the tangential vector $\hat{t}$ of a central ray and the tangential vector of a vicinity ray in the $\hat{t} - \hat{e}_i$ plane. q_i is the distance between the central ray and the vicinity ray in the $\hat{t} - \hat{e}_i$ plane at S.

Figure 3

The ray centered coordinates (s, q_i) and the wavefront coordinates $(s, \tilde{q}_i)$: The Jacobian J between two coordinates is given in equation (46). The curvature K_i and the radius of the curvature R_i of the wavefront are described in terms of η_i and q_i. q_i' is the normal distance between B and C.

Figure 4

A laterally homogeneous velocity model. The gradient of the velocity has a discontinuity at z=10 Km.

Figure 5

Ray trajectories in the model shown in figure 4. The triplication zone is located in the range x=32.4-48.3 Km.

Figure 6

The vertical component VRT seismograms for the model. The center frequency of a narrow band Gaussian source wavelet is 10 Hz, and the receivers are located at the surface (z=0 Km).

Figure 7

The vertical component WKBJ seismograms for the model for 10 Hz. The conditions are the same as in the VRT seismograms in figure 6 except that the WKBJ seismograms were first synthesized for a delta source-time function and then convolved with a narrow band Gaussian wavelet.

Figure 1

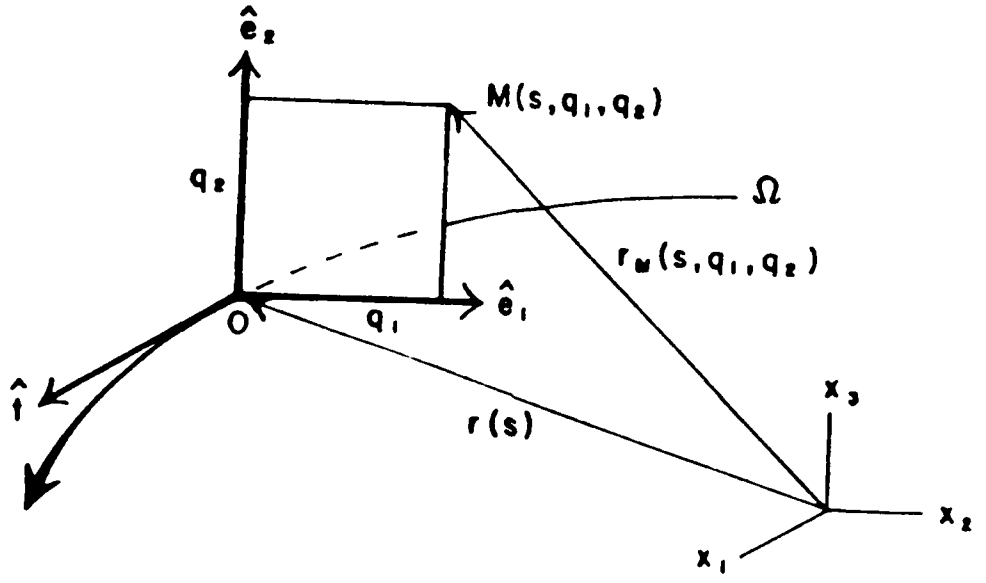

Figure 2

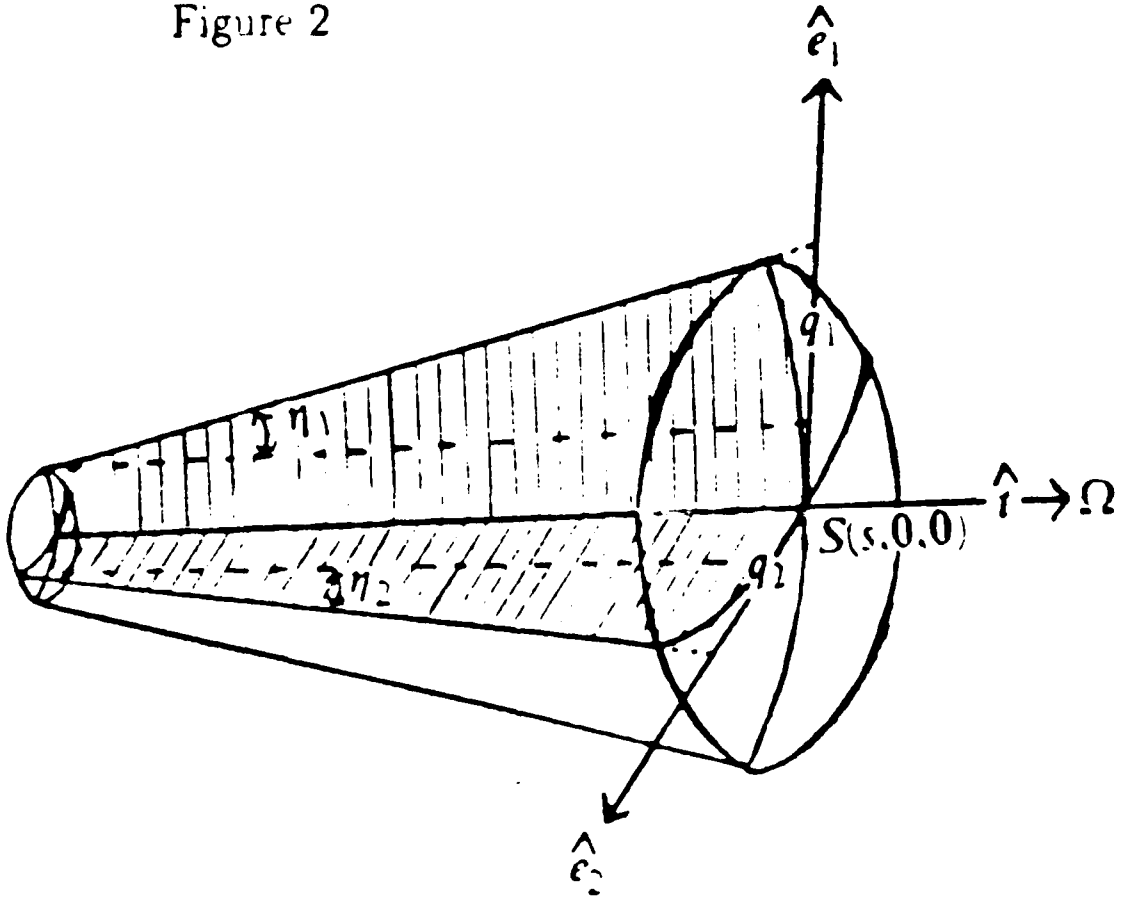

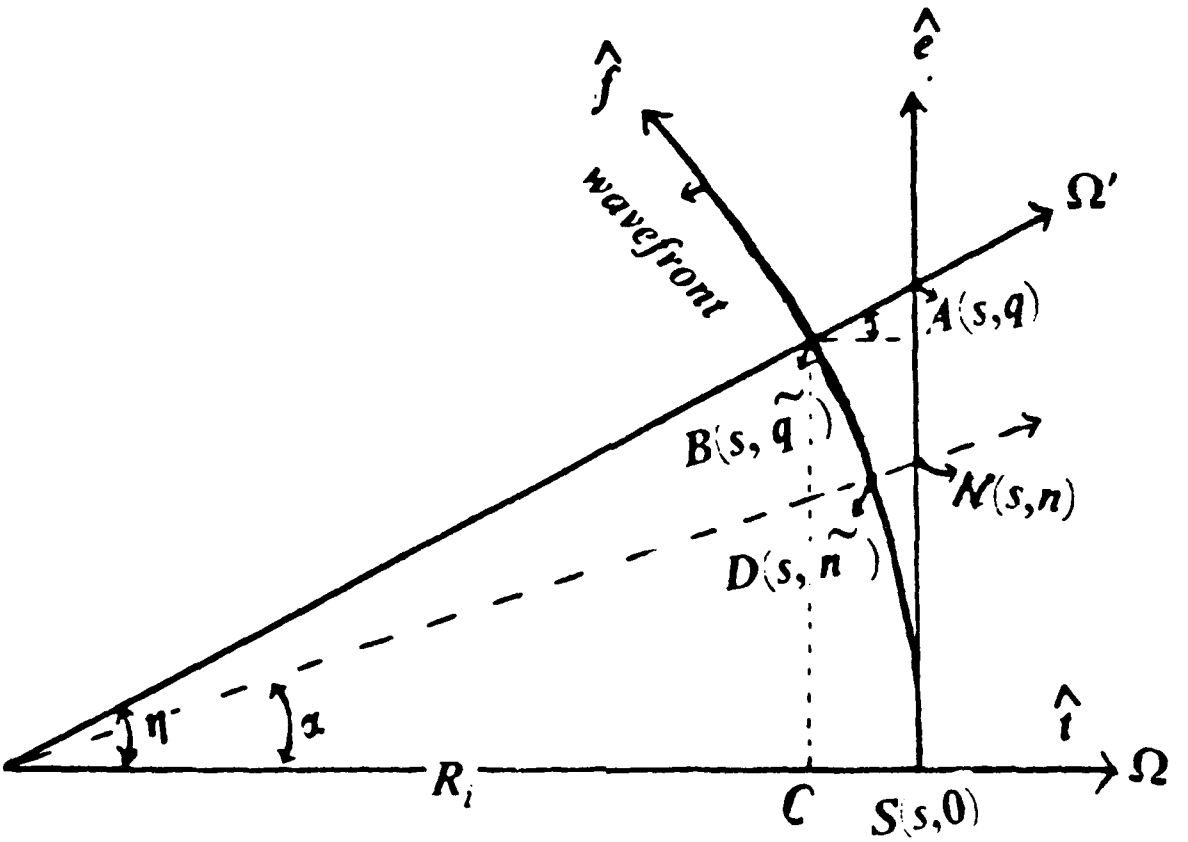

Figure 3

Figure 4: Velocity Structure

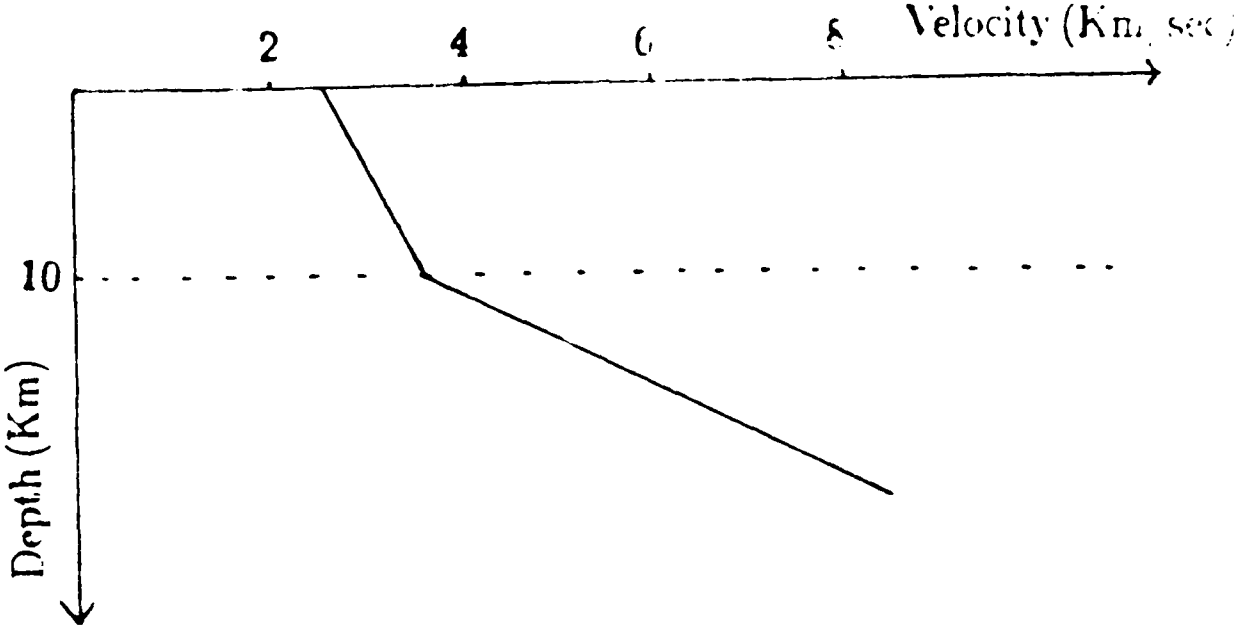

Figure 5. Ray Tracing

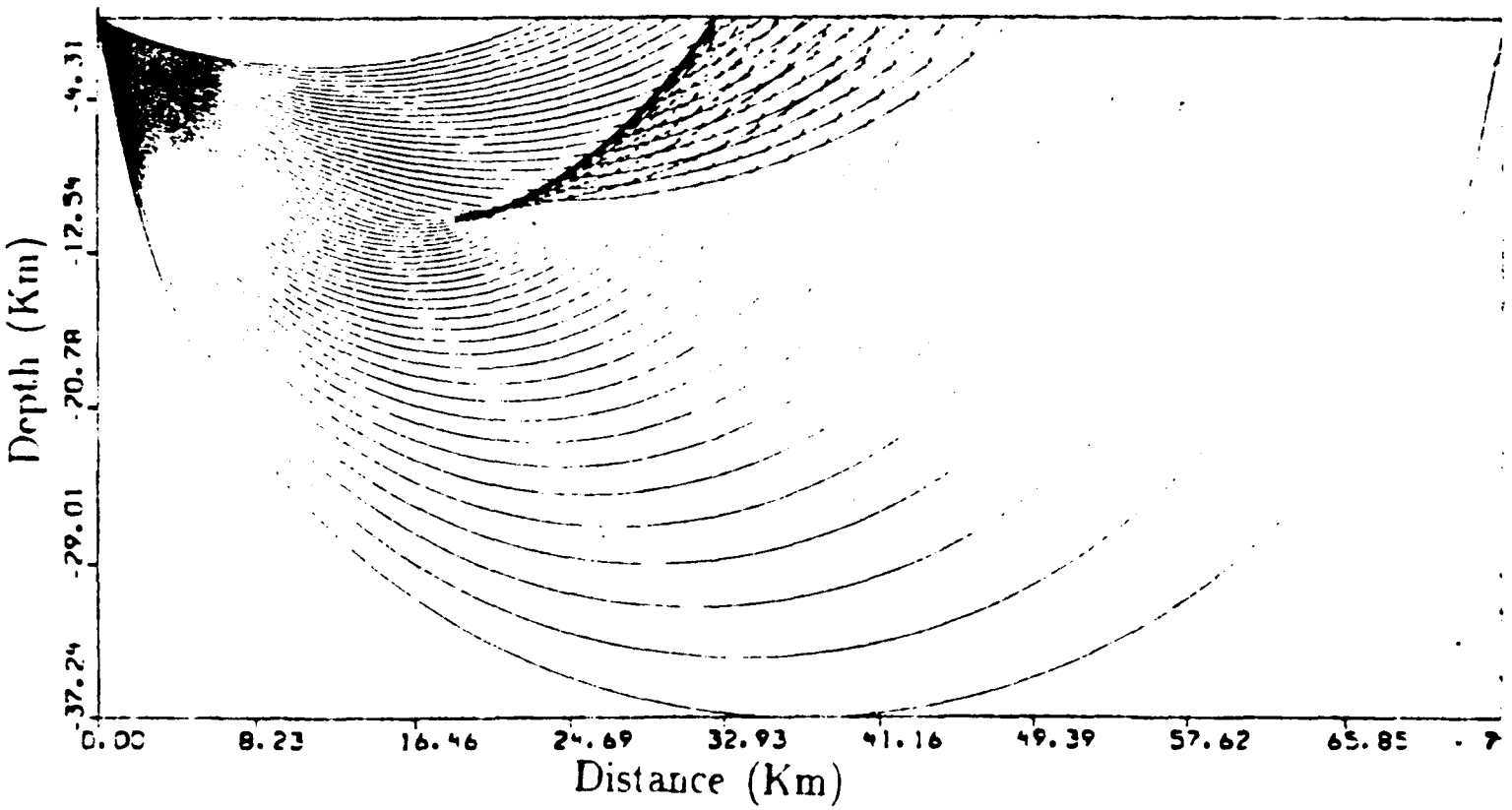

Figure 6: Synthetic Seismograms (5 Hz, VRT)

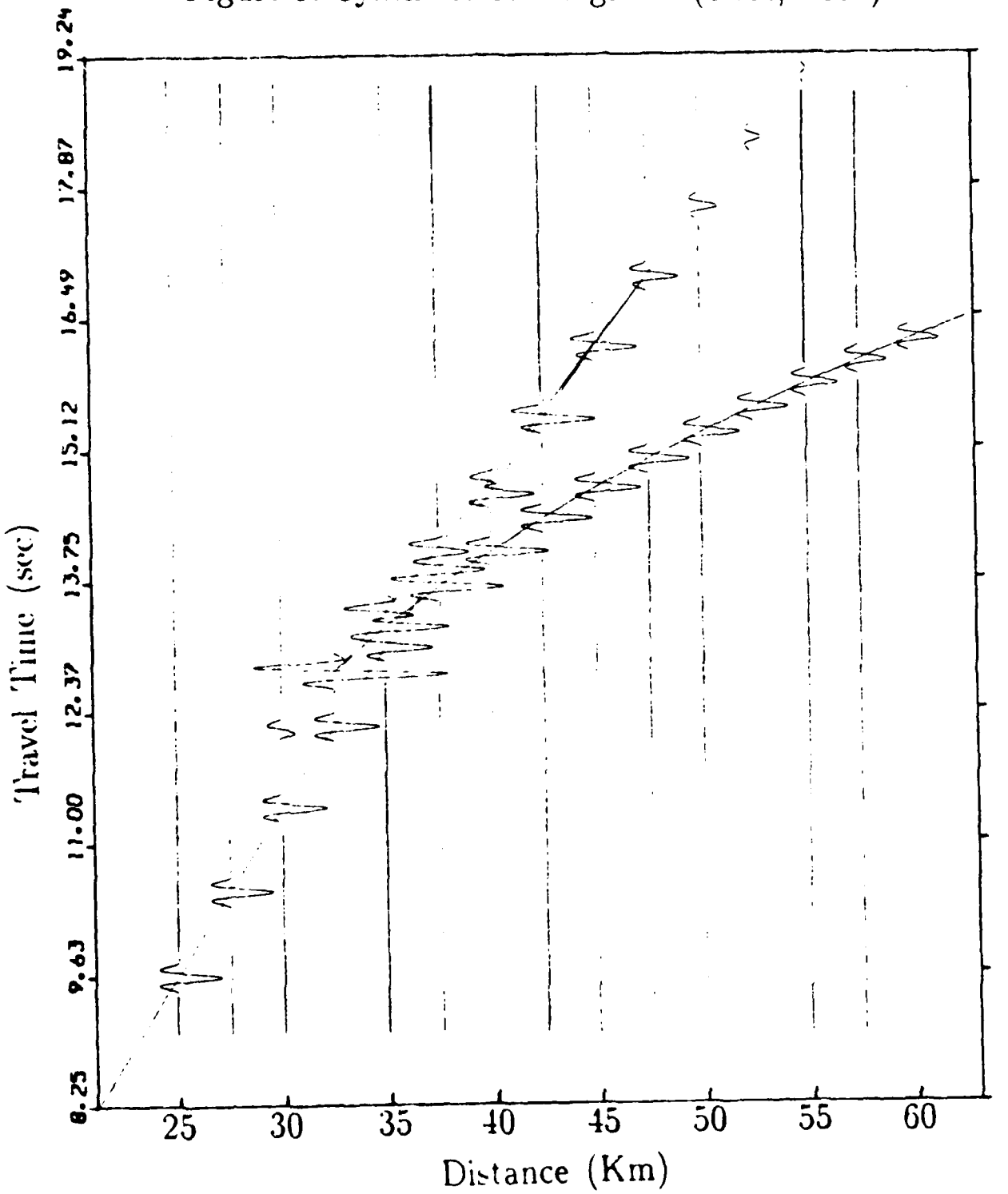

Figure 7: Synthetic Seismograms (5 Hz, WKBJ)

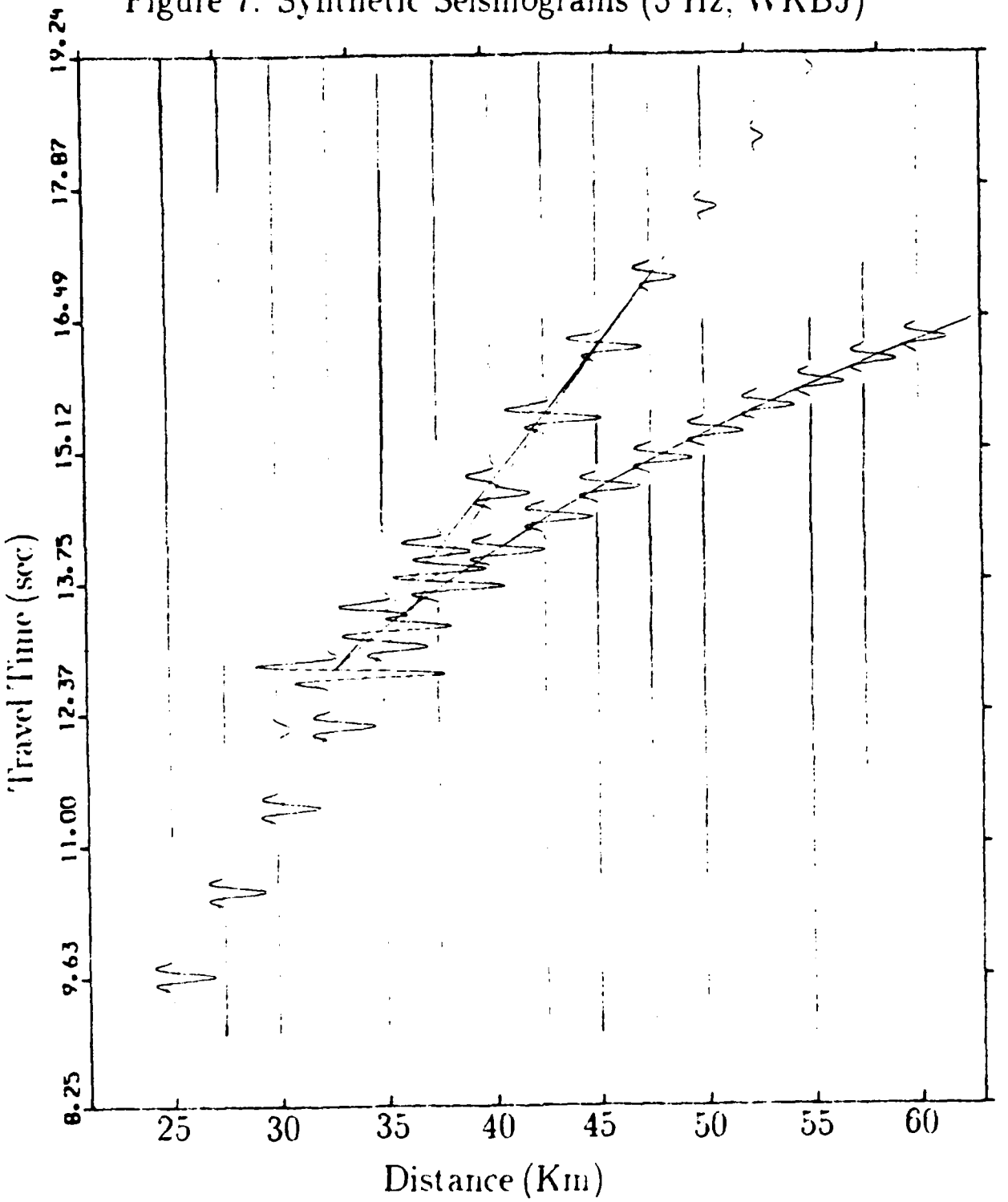

CONTRACTORS (United States)

Professor Keiiti Aki
Center for Earth Sciences
University of Southern California
University Park
Los Angeles, CA 90089-0741

Professor Thomas Ahrens
Seismological Lab, 252-21
Div. of Geological and Planetary
Sciences
California Institute of Technology
Pasadena, CA 91125

Professor Charles B. Archambeau
Cooperative Institute for Resch
in Environmental Sciences
University of Colorado
Boulder, CO 80309

Dr. Thomas C. Bache Jr.
Science Applications Int'l Corp.
10210 Campus Point Drive
San Diego, CA 92121 (2 copies)

Dr. Muawia Barazangi
Institute for the Study of
of the Continent
Cornell University
Ithaca, NY 14853

Dr. Douglas R. Baumgardt
Signal Analysis & Systems Div.
ENSCO, Inc.
5400 Port Royal Road
Springfield, VA 22151-2388

Dr. Jonathan Berger
Institute of Geophysics and
Planetary Physics
Scripps Institution of Oceanography
A-025
University of California, San Diego
La Jolla, CA 92093

Dr. S. Bratt
Science Applications Int'l Corp.
10210 Campus Point Drive
San Diego, CA 92121

Dr. Lawrence J. Burdick
Woodward-Clyde Consultants
P.O. Box 93245
Pasadena, CA 91109-3245 (2 copies)

Professor Robert W. Clayton
Seismological Laboratory/Div. of
Geological & Planetary Sciences
California Institute of Technology
Pasadena, CA 91125

Dr Karl Coyner
New England Research, Inc.
76 Olcott Drive
White River Junction, VT 05001

Dr. Vernon F. Cormier
Department of Geology & Geophysics
U-45, Room 207
The University of Conneticut
Storrs, Connecticut 06268

Dr. Steven Day
Dept. of Geological Sciences
San Diego State U.
San Diego, CA 92182

Dr. Zoltan A. Der
ENSCO, Inc.
5400 Port Royal Road
Springfield, VA 22151-2388

Professor John Ferguson
Center for Lithospheric Studies
The University of Texas at Dallas
P.O. Box 830688
Richardson, TX 75083-0688

Professor Stanley Flatte'
Applied Sciences Building
University of California,
Santa Cruz, CA 95064

Dr. Alexander Florence
SRI International
333 Ravenswood Avenue
Menlo Park, CA 94025-3493

Professor Steven Grand
University of Texas at Austin
Dept of Geological Sciences
Austin, TX 78713-7909

Dr. Henry L. Gray
Associate Dean of Dedman College
Department of Statistical Sciences
Southern Methodist University
Dallas, TX 75275

Professor Roy Greenfield
Geosciences Department
403 Deike Building
The Pennsylvania State University
University Park, PA 16802

Professor David G. Harkrider
Seismological Laboratory
Div of Geological & Planetary Sciences
California Institute of Technology
Pasadena, CA 91125

Professor Donald V. Helmberger
Seismological Laboratory
Div of Geological & Planetary Sciences
California Institute of Technology
Pasadena, CA 91125

Professor Eugene Herrin
Institute for the Study of Earth
and Man/Geophysical Laboratory
Southern Methodist University
Dallas, TX 75275

Professor Robert B. Herrmann
Department of Earth & Atmospheric
Sciences
Saint Louis University
Saint Louis, MO 63156

Professor Bryan Isacks
Cornell University
Dept of Geological Sciences
SNEE Hall
Ithaca, NY 14850

Professor Lane R. Johnson
Seismographic Station
University of California
Berkeley, CA 94720

Professor Thomas H. Jordan
Department of Earth, Atmospheric
and Planetary Sciences
Mass Institute of Technology
Cambridge, MA 02139

Dr. Alan Kafka
Department of Geology &
Geophysics
Boston College
Chestnut Hill, MA 02167

Professor Leon Knopoff
University of California
Institute of Geophysics
& Planetary Physics
Los Angeles, CA 90024

Professor Charles A. Langston
Geosciences Department
403 Deike Building
The Pennsylvania State University
University Park, PA 16802

Professor Thorne Lay
Department of Geological Sciences
1006 C.C. Little Building
University of Michigan
Ann Arbor, MI 48109-1063

Dr. Randolph Martin III
New England Research, Inc.
76 Olcott Drive
White River Junction, VT 05001

Dr. Gary McCartor
Mission Research Corp.
735 State Street
P.O. Drawer 719
Santa Barbara, CA 93102 (2 copies)

Professor Thomas V. McEvilly
Seismographic Station
University of California
Berkeley, CA 94720

Dr. Keith L. McLaughlin
S-CUBED,
A Division of Maxwell Laboratory
P.O. Box 1620
La Jolla, CA 92038-1620

Professor William Menke
Lamont-Doherty Geological Observatory
of Columbia University
Palisades, NY 10964

Professor Brian J. Mitchell
Department of Earth & Atmospheric
Sciences
Saint Louis University
Saint Louis, MO 63156

Mr. Jack Murphy
S-CUBED
A Division of Maxwell Laboratory
11800 Sunrise Valley Drive
Suite 1212
Reston, VA 22091 (2 copies)

Professor J. A. Orcutt
IGPP, A-205
Scripps Institute of Oceanography
Univ. of California, San Diego
La Jolla, CA 92093

Professor Keith Priestley
University of Nevada
Mackay School of Mines
Reno, NV 89557

Professor Paul G. Richards
Lamont-Doherty Geological
Observatory of Columbia Univ.
Palisades, NY 10964

Wilmer Rivers
Teledyne Geotech
314 Montgomery Street
Alexandria, VA 22314

Dr. Alan S. Ryall, Jr.
Center of Seismic Studies
1300 North 17th Street
Suite 1450
Arlington, VA 22209-2308 (4 copies)

Professor Charles G. Sammis
Center for Earth Sciences
University of Southern California
University Park
Los Angeles, CA 90089-0741

Professor Christopher H. Scholz
Geological Sciences
Lamont-Doherty Geological Observatory
Palisades, NY 10964

Dr. Jeffrey L. Stevens
S-CUBED,
A Division of Maxwell Laboratory
P.O. Box 1620
La Jolla, CA 92038-1620

Professor Brian Stump
Institute for the Study of Earth & Man
Geophysical Laboratory
Southern Methodist University
Dallas, TX 75275

Professor Ta-liang Teng
Center for Earth Sciences
University of Southern California
University Park
Los Angeles, CA 90089-0741

Dr. Clifford Thurber
State University of New York at
Stony Brooks
Dept of Earth and Space Sciences
Stony Brook, NY 11794-2100

Professor M. Nafi Toksoz
Earth Resources Lab
Dept of Earth, Atmospheric and
Planetary Sciences
Massachusetts Institute of Technology
42 Carleton Street
Cambridge, MA 02142

Professor Terry C. Wallace
Department of Geosciences
Building #77
University of Arizona
Tucson, AZ 85721

Weidlinger Associates
ATTN: Dr. Gregory Wojcik
4410 El Camino Real, Suite 110
Los Altos, CA 94022

Professor Francis T. Wu
Department of Geological Sciences
State University of New York
at Binghamton
Vestal, NY 13901

OTHERS (United States)

Dr. Monem Abdel-Gawad
Rockwell International Science Center
1049 Camino Dos Rios
Thousand Oaks, CA 91360

Professor Shelton S. Alexander
Geosciences Department
403 Deike Building
The Pennsylvania State University
University Park, PA 16802

Dr. Ralph Archuleta
Department of Geological Sciences
Univ. of California at Santa Barbara
Santa Barbara, CA

J. Barker
Department of Geological Sciences
State University of New York at Binghamton
Vestal, NY 13901

Mr. William J. Best
907 Westwood Drive
Vienna, VA 22180

Dr. N. Biswas
Geophysical Institute
University of Alaska
Fairbanks, AK 99701

Dr. G. A. Bollinger
Department of Geological Sciences
Virginia Polytechnical Institute
21044 Derring Hall
Blacksburg, VA 24061

Mr. Roy Burger
1221 Serry Rd.
Schenectady, NY 12309

Dr. Robert Burridge
Schlumberger-Doll Resch Ctr.
Old Quarry Road
Ridgefield, CT 06877

Science Horizons, Inc.
ATTN: Dr. Theodore Cherry
710 Encinitas Blvd., Suite 101
Encinitas, CA 92024 (2 copies)

Professor Jon F. Claerbout
Professor Amos Nur
Dept. of Geophysics
Stanford University
Stanford, CA 94305 (2 copies)

Dr. Anton W. Dainty
AFGL/LWH
Hanscom AFB, MA 01731

Professor Adam Dziewonski
Hoffman Laboratory
Harvard University
20 Oxford St.
Cambridge, MA 02138

Professor John Ebel
Dept of Geology and Geophysics
Boston College
Chestnut Hill, MA 02167

Dr. Donald Forsyth
Dept of Geological Sciences
Brown University
Providence, RI 02912

Dr. Anthony Gangi
Texas A&M University
Department of Geophysics
College Station, TX 77843

Dr. Freeman Gilbert
Institute of Geophysics & Planetary Physics
University of California, San Diego
P.O. Box 109
La Jolla, CA 92037

Mr. Edward Giller
Pacific Seirra Research Corp.
1401 Wilson Boulevard
Arlington, VA 22209

Dr. Jeffrey W. Given
Sierra Geophysics
11255 Kirkland Way
Kirkland, WA 98033

Rong Song Jih
Teledyne Geotech
314 Montgomery Street
Alexandria, Virginia 22314

Professor F.K. Lamb
University of Illinois at
Urbana-Champaign
Department of Physics
1110 West Green Street
Urbana, IL 61801

Dr. Arthur Lerner-Lam
Lamont-Doherty Geological Observatory
of Columbia University
Palisades, NY 10964

Dr. L. Timothy Long
School of Geophysical Sciences
Georgia Institute of Technology
Atlanta, GA 30332

Dr. Peter Malin
University of California at
Santa Barbara
Institute for Central Studies
Santa Barbara, CA 93106

Dr. George R. Mellman
Sierra Geophysics
11255 Kirkland Way
Kirkland, WA 98033

Dr. Bernard Minster
IGPP, A-205
Scripps Institute of Oceanography
Univ. of California, San Diego
La Jolla, CA 92093

Professor John Nabelek
College of Oceanography
Oregon State University
Corvallis, OR 97331

Dr. Geza Nagy
U. California, San Diego
Dept of Ames, M.S. B-010
La Jolla, CA 92093

Dr. Jack Oliver
Department of Geology
Cornell University
Ithaca, NY 14850

Dr. Robert Phinney/Dr. F. A. Dahlen
Dept of Geological
Geological Science University
Princeton University
Princeton, NJ 08540

RADIX System, Inc.
Attn: Dr. Jay Pulli
2 Taft Court, Suite 203
Rockville, Maryland 20850

Dr. Norton Rimer
S-CUBED
A Division of Maxwell Laboratory
P.O. 1620
La Jolla, CA 92038-1620

Professor Larry J. Ruff
Department of Geological Sciences
1006 C.C. Little Building
University of Michigan
Ann Arbor, MI 48109-1063

Dr. Richard Sailor
TASC Inc.
55 Walkers Brook Drive
Reading, MA 01867

Thomas J. Sereno, Jr.
Service Application Int'l Corp.
10210 Campus Point Drive
San Diego, CA 92121

Dr. David G. Simpson
Lamont-Doherty Geological Observ.
of Columbia University
Palisades, NY 10964

Dr. Bob Smith
Department of Geophysics
University of Utah
1400 East 2nd South
Salt Lake City, UT 84112

Dr. S. W. Smith
Geophysics Program
University of Washington
Seattle, WA 98195

Dr. Stewart Smith
IRIS Inc.
1616 N. Fort Myer Drive
Suite 1440
Arlington, VA 22209

Rondout Associates
ATTN: Dr. George Sutton,
Dr. Jerry Carter, Dr. Paul Pomeroy
P.O. Box 224
Stone Ridge, NY 12484 (4 copies)

Dr. L. Sykes
Lamont Doherty Geological Observ.
Columbia University
Palisades, NY 10964

Dr. Pradeep Talwani
Department of Geological Sciences
University of South Carolina
Columbia, SC 29208

Dr. R. B. Tittmann
Rockwell International Science Center
1049 Camino Dos Rios
P.O. Box 1085
Thousand Oaks, CA 91360

Professor John H. Woodhouse
Hoffman Laboratory
Harvard University
20 Oxford St.
Cambridge, MA 02138

Dr. Gregory B. Young
ENSCO, Inc.
5400 Port Royal Road
Springfield, VA 22151-2388

FOREIGN (OTHERS)

Dr. Peter Basham
Earth Physics Branch
Geological Survey of Canada
1 Observatory Crescent
Ottawa, Ontario
CANADA K1A 0Y3

Professor Ari Ben-Menahem
Dept of Applied Mathematics
Weizman Institute of Science
Rehovot
ISRAEL 951729

Dr. Eduard Berg
Institute of Geophysics
University of Hawaii
Honolulu, HI 96822

Dr. Michel Bouchon - Universite
Scientifique et Medicale de Grenob
Lab de Geophysique - Interne et
Tectonophysique - I.R.I.G.M-B.P.
38402 St. Martin D'Heres
Cedex FRANCE

Dr. Hilmar Bungum/NTNF/NORSAR
P.O. Box 51
Norwegian Council of Science,
Industry and Research, NORSAR
N-2007 Kjeller, NORWAY

Dr. Michel Campillo
I.R.I.G.M.-B.P. 68
38402 St. Martin D'Heres
Cedex, FRANCE

Dr. Kin-Yip Chun
Geophysics Divlsion
Physics Department
University of Toronto
Ontario, CANADA M5S 1A7

Dr. Alan Douglas
Ministry of Defense
Blacknest, Brimpton,
Reading RG7-4RS
UNITED KINGDOM

Dr. Manfred Henger
Fed. Inst. For Geosciences & Nat'l Res.
Postfach 510153
D-3000 Hannover 51
FEDERAL REPUBLIC OF GERMANY

Ms. Eva Johannisson
Senior Research Officer
National Defense Research Inst.
P.O. Box 27322
S-102 54 Stockholm
SWEDEN

Tormod Kvaerna
NTNF/NORSAR
P.O. Box 51
N-2007 Kjeller, NORWAY

Mr. Peter Marshall, Procurement
Executive, Ministry of Defense
Blacknest, Brimpton,
Reading FG7-4RS
UNITED KINGDOM (3 copies)

Dr. Robert North
Geophysics Division
Geological Survey of Canada
1 Observatory crescent
Ottawa, Ontario
CANADA, K1A 0Y3

Dr. Frode Ringdal
NTNF/NORSAR
P.O. Box 51
N-2007 Kjeller, NORWAY

Dr. Jorg Schlittenhardt
Federal Inst. for Geosciences & Nat'l Res.
Postfach 510153
D-3000 Hannover 51
FEDERAL REPUBLIC OF GERMANY

University of Hawaii
Institute of Geophysics
ATTN: Dr. Daniel Walker
Honolulu, HI 96822

FOREIGN CONTRACTORS

Dr. Ramon Cabre, S.J.
Observatorio San Calixto
Casilla 5939
La Paz Bolivia

Professor Peter Harjes
Institute for Geophysik
Rhur University/Bochum
P.O. Box 102148, 4630 Bochum 1
FEDERAL REPUBLIC OF GERMANY

Dr. E. Husebye
NTNF/NORSAR
P.O. Box 51
N-2007 Kjeller, NORWAY

Professor Brian L.N. Kennett
Research School of Earth Sciences
Institute of Advanced Studies
G.P.O. Box 4
Canberra 2601
AUSTRALIA

Dr. B. Massinon
Societe Radiomana
27, Rue Claude Bernard
7,005, Paris, FRANCE (2 copies)

Dr. Pierre Mechler
Societe Radiomana
27, Rue Claude Bernard
75005, Paris, FRANCE

Dr. Svein Mykkeltveit
NTNF/NORSAR
P.O. Box 51
N-2007 Kjeller, NORWAY (3 copies)

GOVERNMENT

Dr. Ralph Alewine III
DARPA/NMRO
1400 Wilson Boulevard
Arlington, VA 22209-2308

Dr. Robert Blandford
DARPA/NMRO
1400 Wilson Boulevard
Arlington, VA 22209-2308

Sandia National Laboratory
ATTN: Dr. H. B. Durham
Albuquerque, NM 87185

Dr. Jack Evernden
USGS-Earthquake Studies
345 Middlefield Road
Menlo Park, CA 94025

U.S. Geological Survey
ATTN: Dr. T. Hanks
Nat'l Earthquake Resch Center
345 Middlefield Road
Menlo Park, CA 94025

Dr. James Hannon
Lawrence Livermore Nat'l Lab.
P.O. Box 808
Livermore, CA 94550

Paul Johnson
ESS-4, Mail Stop J979
Los Alamos National Laboratory
Los Alamos, NM 87545

Ms. Ann Kerr
DARPA/NMRO
1400 Wilson Boulevard
Arlington, VA 22209-2308

Dr. Max Koontz
US Dept of Energy/DP 5
Forrestal Building
1000 Independence Ave.
Washington, D.C. 20585

Dr. W. H. K. Lee
USGS
Office of Earthquakes, Volcanoes,
& Engineering
Branch of Seismology
345 Middlefield Rd
Menlo Park, CA 94025

Dr. William Leith
U.S. Geological Survey
Mail Stop 928
Reston, VA 22092

Dr. Richard Lewis
Dir. Earthquake Engineering and
Geophysics
U.S. Army Corps of Engineers
Box 631
Vicksburg, MS 39180

Dr. Robert Masse'
Box 25046, Mail Stop 967
Denver Federal Center
Denver, Colorado 80225

Richard Morrow
ACDA/VI
Room 5741
320 21st Street N.W.
Washington, D.C. 20451

Dr. Keith K. Nakanishi
Lawrence Livermore National Laboratory
P.O. Box 808, L-205
Livermore, CA 94550 (2 copies)

Dr. Carl Newton
Los Alamos National Lab.
P.O. Box 1663
Mail Stop C335, Group ESS-3
Los Alamos, NM 87545

Dr. Kenneth H. Olsen
Los Alamos Scientific Lab.
P.O. Box 1663
Mail Stop C335, Group ESS-3
Los Alamos, NM 87545

Howard J. Patton
Lawrence Livermore National
Laboratory
P.O. Box 808, L-205
Livermore, CA 94550

Mr. Chris Paine
Office of Senator Kennedy
SR 315
United States Senate
Washington, D.C. 20510

AFOSR/NP
ATTN: Colonel Jerry J. Perrizo
Bldg 410
Bolling AFB, Wash D.C. 20332-6448

HQ AFTAC/TT
Attn: Dr. Frank F. Pilotte
Patrick AFB, Florida 32925-6001

Mr. Jack Rachlin
USGS - Geology, Rm 3 C136
Mail Stop 928 National Center
Reston, VA 22092

Robert Reinke
AFWL/NTESG
Kirtland AFB, NM 87117-6008

Dr. Byron Ristvet
HQ DNA, Nevada Operations Office
Attn: NVCG
P.O. Box 98539
Las Vegas, NV 89193

HQ AFTAC/TGR
Attn: Dr. George H. Rothe
Patrick AFB, Florida 32925-6001

Donald L. Springer
Lawrence Livermore National Laboratory
P.O. Box 808, L-205
Livermore, CA 94550

Dr. Lawrence Turnbull
OSWR/NED
Central Intelligence Agency
CIA, Room 5G48
Washington, D.C. 20505

Dr. Thomas Weaver
Los Alamos National Laboratory
P.O. Box 1663
MS C 335
Los Alamos, NM 87545

GL/SULL
Research Library
Hanscom AFB, MA 01731-5000 (2 copies)

Secretary of the Air Force (SAFRD)
Washington, DC 20330
Office of the Secretary Defense
DDR & E
Washington, DC 20330

HQ DNA
ATTN: Technical Library
Washington, DC 20305

DARPA/RMO/RETRIEVAL
1400 Wilson Blvd.
Arlington, VA 22209

DARPA/RMO/Security Office
1400 Wilson Blvd.
Arlington, VA 22209

GL/XO
Hanscom AFB, MA 01731-5000

GL/LW
Hanscom AFB, MA 01731-5000

DARPA/PM
1400 Wilson Boulevard
Arlington, VA 22209

Defense Technical
Information Center
Cameron Station
Alexandria, VA 22314
(5 copies)

Defense Intelligence Agency
Directorate for Scientific &
Technical Intelligence
Washington, D.C. 20301

Defense Nuclear Agency/SPSS
ATTN: Dr. Michael Shore
6801 Telegraph Road
Alexandria, VA 22310

AFTAC/CA (STINFO)
Patrick AFB, FL 32925-6001

Dr. Gregory van der Vink
Congress of the United States
Office of Technology Assessment
Washington, D.C. 20510

Mr. Alfred Lieberman
ACDA/VI-OA'State Department Building
Room 5726
320 - 21St Street, NW
Washington, D.C. 20451

TACTEC
Battelle Memorial Institute
505 King Avenue
Columbus, OH 43201 (Final report only)